Towards Net-Zero Sustainable Aviation Fuel with Wet Waste-Derived Volatile Fatty Acids

Nabila A. Huq,[a] Glenn R. Hafenstine,[a] Xiangchen Huo,[a] Hannah Nguyen,[a] Stephen M. Tifft,[a] Davis R. Conklin,[a] Daniela Stück,[a] Jim Stunkel,[a] Zhibin Yang,[b] Joshua S. Heyne,[b] Matthew R. Wiatrowski,[a] Yimin Zhang,[a] Ling Tao,[a] Junqing Zhu,[c] Charles S. McEnally,[c] Earl D. Christensen,[a] Cameron Hays,[a] Kurt M. Van Allsburg,[a] Kinga A. Unocic,[d] Harry M. Meyer III,[e] Zia Abdullah,[a] Derek R. Vardon[a]*

[a]*Catalytic Carbon Transformation Center, National Renewable Energy Laboratory, Golden, CO 80401, USA*
[b]*Mechanical and Aerospace Engineering, University of Dayton, Dayton, OH 45469, USA.*
[c]*Chemical and Environmental Engineering, Yale University, New Haven, CT 06520, USA.*
[d]*Center for Nanophase Materials Sciences, Oak Ridge National Laboratory, Oak Ridge, TN, USA.*
[e]*Chemical Sciences Division, Oak Ridge National Laboratory, Oak Ridge, TN, USA.*

*Corresponding author. *Email: Derek.Vardon@nrel.gov. Phone: 303-384-7763*

Section S1: Materials and Methods

Materials

VFAs derived from Food Waste. VFAs derived from food waste were provided by Earth Energy Renewables using their integrated fermentation and VFA recovery pilot facility. In brief, VFAs were produced by arrested anaerobic digestion using mixed microbial consortia. The fermentation was performed at mesophilic temperatures under conditions which suppressed methane formation. Carbon dioxide and residual solids containing cell mass and indigestible organic matter are the two main byproducts from fermentation. Fermentation broth was processed online to recover highly pure $\geq C_3$ VFAs using a proprietary extraction and distillation process that alleviates the need to form VFA salts with caustic addition for recovery. C_2 VFA, process water, and caustic were recycled back to fermentation continuously. Recovered VFAs from two food waste fermentation runs were provided, with each run containing two fractions comprised of C_3-C_5 VFAs and $\geq C_6$ VFAs. The average VFA mass yield from food waste was 0.45 kg VFA/kg dry food waste, as discussed in the Techno-Economic Analysis section below. Further information on emerging VFA production and separation technologies can be found within literature (1-6).

Once received at NREL, prior to catalytic upgrading VFA fractions were filtered through a 0.45-µm Nylon membrane vacuum filter from GVS Filter Technology and combined to produce three samples with varying VFA compositional profiles. This included a predominantly C_4 VFA sample, C_4/C_6 VFA sample, and C_6/C_8 VFA sample, as shown in **Table S3**. No additional pretreatment steps were performed on the VFA samples prior to catalytic testing and VFA samples were processed neat for ketonization.

Model VFAs. Model VFAs were purchased from Sigma Aldrich to mimic biogenic VFA profiles. Samples were used as received.

Catalyst Materials. ZrO_2 pellets were obtained from Johnson Matthey. Pellets were crushed and sieved to 30-50 mesh particles, and calcinated in stagnant air at 500°C for 2 h before use (5 °C/min ramp to temperature). Niobic acid hydrate (HY-340) was obtained from CBMM and used as received. Pt/Al_2O_3 catalyst was prepared with chloroplatinic acid hexahydrate obtained from Sigma Aldrich and Al_2O_3 pellets obtained from Alfa Aesar.

Fossil Jet Fuel. The fossil jet fuel used as a blending base fuel was required to represent an "average" aviation fuel with respect to physical and chemical properties. The selected POSF 10325 Jet A was source directly from the Shell Mobile without exposure to the pipeline infrastructure. Its carbon number distribution is shown in **Table S6**.

Methods

VFA Characterization

Water content of VFA samples was determined using Karl-Fischer titration on a Metrohm 870 KF Titrino plus using the Aquastar CombiTitrant 5 solvent. Inductively coupled plasma mass spectrometry was performed by Huffman Hazen Laboratories to determine impurity concentrations for several elements in VFA, ketone and hydrocarbon samples.

Simplified Kinetic Model for VFA Ketonization

The ketone product distribution was predicted using a simplified kinetic model for VFA ketonization at nearly 100% conversion of all the acids. The model was generalized for a reaction network of n-VFAs. Each unique VFA composition (including number of reactants, acid chain length, and acid concentration) is the model input and ketone distribution is model output. Reaction rate order of two was assumed since the rate limiting step of the acid ketonization was proposed to be the coupling of the two adsorbed acid molecules (7). The rate of a ketonization between two VFAs is described by **Eqn. S1**. The set of differential equations in **Eqn. S2-S4** was solved with ode45 in Matlab for the temporal profiles of the acids, ketones, CO_2 and H_2O by products.

$$r_{ij} = k_{ij} C_{acid_i} C_{acid_j} \quad \text{(Eqn. S1)}$$

$$\frac{dC_{acid_i}}{dt} = \frac{dC_{acid_j}}{dt} = -r_{ij} \quad \text{If } i \neq j \quad \text{(Eqn. S2)}$$

$$\frac{dC_{acid_i}}{dt} = \frac{dC_{acid_j}}{dt} = -2r_{ij} \quad \text{If } i = j \quad \text{(Eqn. S3)}$$

$$\frac{dC_{ketone_{ij}}}{dt} = r \quad \text{(Eqn. S4)}$$

Whereas k_{ij} is the rate constant of ketonization between $acid_i$ and $acid_j$, and C_{acid} is the concentration (mol/L) of the acid reactant, $C_{ketoneij}$ is the concentration of ketone product from reaction of $acid_i$ and $acid_j$. For each ketonization reaction, the amount of water or CO_2 formed is equal to that of the ketone. We assume that $k_{ij} = 2k_{ii}$. Because it has been reported that the rate constant for cross-ketonization ($i \neq j$) is double that for self-ketonization ($i = j$) (8).

HDO Catalyst Synthesis

Pt/Al_2O_3 catalyst was prepared by strong electrostatic adsorption method with chloroplatinic acid hexahydrate as Pt precursor. Al_2O_3 of 30-50 mesh (crushed and sieved from Alfa Aesar Al_2O_3 pellets) and Pt precursor were added to deionized water, and solution pH was adjusted to 3 by adding HCl. After stirring overnight, the catalyst particles were recovered by filtration extensively washed with deionized water. The catalyst was dried in the air and reduced in flowing H_2 (200 mL min^{-1}) at 300°C for 4 h prior to use.

Estimation of Catalyst Costs

A cost estimate for the ZrO_2 extrudate ketonization catalyst was developed using CatCost v1.0.4 (9) and its Step Method for estimating the cost of contract manufacture (10). Since this method produces highly scale-dependent costs that would likely overestimate the cost of the small catalyst charge (167 kg) used in the modeled biorefinery, it was assumed that an off-the-shelf ZrO_2 extrudate would be available at a lower cost than that for a custom catalyst from a contract manufacturer. Starting from commercial zirconia powder ($26/kg) and performing an extrusion step, initial rough estimates informed an assumed cost for an off-the-shelf catalyst formulation of $50/kg, with $30/kg and $90/kg as low and high cost scenarios. Costs for the HDO catalyst (3% Pt/Al_2O_3) are consistent with literature (11). Alternative HDO catalyst formulations of 9% Co or 7% Ni on a Perlkat amorphous silica-alumina support(12) were also evaluated and gave costs ca. $10–35/kg in the order size range of 5–500 tons.

Catalyst Characterization

Physisorption. Nitrogen physisorption was performed using a Quadrasorb evo (Quantachrome). In a typical measurement, 0.10 g of catalyst was degassed under flowing He at 200 °C for 16 h. Full adsorption and desorption isotherms were recorded for each sample at -196 °C (77 K). Surface area was computed using the multi-point Brunauer-Emmett-Teller (BET) method, while pore volume and pore size distribution were determined using the Barrett, Joyner and Halenda (BJH) method for the desorption isotherm.

NH_3 temperature programmed desorption. Temperature programmed desorption (TPD) of NH_3 was performed using an Autochem II 2920 (Micromeritics) to measure catalyst acidity (**Figure S6**). Approximately 0.10 g of catalyst was loaded into a quartz u-tube and supported by quartz wool. After purging the system with helium, the catalyst was pretreated by ramping to 120 °C for 1 h, then 500 °C for 2 h in flowing helium. After cooling to 120 °C, a stream of premixed 10% NH_3 (balance helium) was passed over the catalyst for 1 h to saturate acidic sites on the catalyst surface. Following a 2-h helium purge at 120 °C to remove physisorbed NH_3, the sample temperature was ramped to 500 °C at 10 °C min^{-1} in helium carrier gas at 50 cm3 (STP) min^{-1}, while NH_3 concentration in the effluent was monitored by a thermal conductivity detector (TCD). After calibrating the TCD, the desorption peak area was used to calculate the total quantity of acid sites by assuming a 1:1 stoichiometry of NH_3 binding to acid sites.

Pyridine diffuse reflectance Fourier transform infrared spectroscopy (DRIFTS). DRIFTS measurements were performed using a Thermo Nicolet iS50 FT-IR spectrometer equipped with a Harrick Praying Mantis

reaction chamber (**Figure S7**). ZrO_2 samples were treated at 350 °C (5 °C min^{-1} ramp) for 2 h under flowing N_2, cooled to 150 °C and purged with N_2 for 10 min before collecting a background spectrum. The samples were then dosed with pyridine vapor by flowing N_2 through a pyridine filled bubbler at room temperature for 5 min before removing physisorbed pyridine under N_2 by heating to 200 °C (5 °C min^{-1} ramp) and holding for 30 min. The samples were cooled back to 150 °C and the spectra were collected by taking 64 scans at a resolution of 4 cm N_2. The background spectra were subtracted from the average spectra before identifying peaks associated with Brønsted and Lewis acid sites.

Thermal Gravimetric Analysis. The irreversibly adsorbed carbon amount of spent catalysts was measured by a Setaram Setsys Evolution thermal gravimetric analyzer (TGA) coupled with a Nicolet 6700 Fourier Transform InfraRed (FTIR) spectrometer via a transfer line heated at 200°C. The FTIR spectrometer is equipped with a gas cell maintained at 225°C to prevent vapor condensation. The catalyst was heated to 800°C under zero air (19-21% oxygen with a balance of nitrogen). The onset of carbon combustion was determined by the observation of carbon dioxide in the FTIR. Prior to the onset of carbon combustion, only water was observed in the FTIR spectra. Therefore, the carbon content was calculated by subtracting the mass loss due to water from the total mass loss recorded by the TGA.

Microscopy. Scanning transmission electron microscopy with energy dispersive X-ray spectroscopy (STEM-EDS) was used to reveal morphology and elemental distribution of fresh, spent and regenerated ZrO_2 catalyst (**Figure S5, S9**). High resolution (HR)-STEM imaging was conducted utilizing an aberration-corrected a JEOL 2200FS STEM/TEM instrument equipped with a CEOS GmbH (Heidelberg, Ger) corrector on the illuminating lenses and operated at 200 kV. The MAG 7C mode was used to achieve a probe with a nominal 41 pA current and associated resolution of a nominal 0.07 nm. STEM-EDS was performed on FEI F200X Talos operating at 200 kV, which is equipped with an extreme field emission gun (X-FEG) electron source, high-angle annular dark-field (HAADF) detector and Super-X EDS system with 4 silicon-drift detectors (SDD) (Bruker XFlash® 6 series with detector size 120 mm^2) with a solid angle of 0.9 Steradian for chemical analysis. To avoid and/or decrease any potential electron beam damage during spectroscopy analysis but maintain high signal-to-noise ratio, the current of the electron beam was controlled and was set to 480 pA. For scanning transmission electron microscopy (STEM) analysis, the catalysts were drop-cast onto lacey carbon-coated copper grids (SPI Supplies part no. Z3820C) from isopropanol suspensions.

X-ray Photoelectron Spectroscopy (XPS). XPS was used to identify the elements that exist on the catalyst surface and to what elements they are bonded to as well as to identify their chemical state. The XPS analysis was performed using a Thermo Scientific K-Alpha XPS instrument using a 400-micron diameter x-ray spot. Three samples, fresh, spent and regenerated ZrO_2, were analyzed. The three powder samples were mounted for analysis by dispersing onto double-sided tape fixed to a clean glass slide. After insertion into the analysis chamber, a wide energy range survey scan was acquired to determine all elements present. Next, a set of narrow energy range core level spectra were acquired for each identified element. The survey data were acquired to obtain the overall surface composition for each sample (**Table S4**). The surface compositions were determined using the core level data. Analysis also involved comparison of the C 1s, O 1s, and Zr 3d core level spectra for the three catalysts to identify the bonding. The C 1s showed at least four type of carbon bonding: C-C; C-O; O=C-O; and a small carbonate feature. O 1s also showed multiple bonding configurations: O-Zr; O=C, and O-C. The Zr 3d was a doublet having both Zr $3d_{5/2}$ and Zr $3d_{3/2}$ spin orbit split pairs. Two distinct forms of Zr were found in fresh ZrO_2; one at Zr $3d_{5/2}$ ~182 eV (assigned to ZrO_2) and one at Zr $3d_{5/2}$ ~183 eV, which is likely related to a surface hydroxide or carbonate. The Zr-O portion was dominant in the spent and regenerated ZrO_2.

Chemical Product Analysis

Gas chromatography. Samples of liquid products were analyzed using gas chromatography on an Agilent 7890 GC system equipped with a Polyarc-flame ionization detector (Polyarc-FID) for quantifying concentrations and a mass spectrometer (MS, Agilent Technologies) for identifying products (**Figures S3, S13-S16**). The instrument utilized an HP-5MS column (30 m x 0.25 4 mm), split injection (25:1), an injection volume of 1 μL, an inlet temperature of 260 °C, ramped under a program (40 °C for 2 min, then 18 °C min^{-1} to 280 C), and helium as the carrier gas at 29 cm sec^{-1}. The eluent from the column was split into the Polyarc-FID and MS instruments for simultaneous measurements. The Polyarc (Advanced Research Company) device catalytically converts organic compounds into methane before traditional FID

to allow for facile concentration measurements for several products in a sample based upon a single standard calibration curve.

Ketonization Flow Reactor

Conversion, Mass Yield and Selectivity. VFA ketonization experiments were performed in a custom built trickle bed flow reactor (Parr) consisting of a mass flow controller (Brooks Instruments) for adjusting the flowrate the argon gas, a high-pressure liquid chromatography pump (Chromtech) for controlling liquid addition, a clamshell furnace for temperature control, a tube-in-tube heat exchanger for condensing liquids from the reactor effluent, and a knock-out pot for collecting liquid product mixtures. All ketonization reactions were performed at atmospheric pressure with no back-pressure regulation. The liquid and gas feeds mixed above the reactor tube (1/2" outer diameter, Dursan-coated stainless steel (SilcoTek Coating Co.) and flowed across the ZrO_2 catalyst bed (30-50 mesh, Johnson Matthey). Liquid samples were analyzed by GC while the effluent gas was analyzed by an online non-dispersive infrared detector for concentrations of CO_2, CO, CH_4 and O_2. Conversion, yield, and selectivity from the ketonization reactions were calculated using the following equations:

$$Conversion = \frac{Mol_{acid,in} - Mol_{acid,out}}{Mol_{acid,in}} \quad \text{(Eqn. S5)}$$

$$Yield\ (mass\ \%) = \frac{Mass_{product,out}}{(Mass_{acid,in})} * 100\% \quad \text{(Eqn. S6)}$$

$$Selectivity\ (\%) = \frac{Yield_{Ketones}}{(Yield_{Ketones} + Yield_{Non-targets})} * 100\% \quad \text{(Eqn. S7)}$$

Post-Ketonization Distillation

The organic phase from the C_4/C_6 ketonization reaction was decanted from the aqueous phase and then distilled in a BR Instruments® Micro-distillation column to separate $\leq C_7$ ketones from $\geq C_8$ ketones. The BR Instruments® Micro-distillation column was run at 45 torr and heated at an initial rate of 10% and increased to 12.5% after the first few milliliters of distillate were collected. The reflux ratio was held at twenty until the first few milliliters of distillate were collected at which point the reflux ratio was decreased to five. The condenser circulating an 80:20 water to ethylene glycol mixture was held at 5°C for the duration of the distillation. A Teflon band rotating 120 rpm was used in the column. The lighter ketones $\leq C_7$ were collected in the distillate from room temperature up to 160°C and utilized for aldol condensation (**Figure S13**) while the heavier ketones $\geq C_8$ were used for subsequent HDO process (**Figure S14**). This process removed all but 7% of C_7 ketones (and all measurable C_4-C_6 ketones) from the heavier fraction and approximately 21% of C_8-C_9 ketones distilled into the light fraction.

Ketonization Catalyst Regeneration

Following 100 h testing with biogenic VFAs, the ZrO_2 catalyst was recovered from the reactor for further characterization and regeneration. Catalyst regeneration conditions were as follows: 5 °C/min to 500 °C, hold 12 h, cool naturally, in flowing air.

Ketone Aldol Condensation

Ketone condensation experiments were performed in a Dean-Stark reactor system. In a 500-mL round-bottom flask, 250 g feed (20 wt% ketone in decane) and 25 g niobic acid hydrate were mixed with a Teflon-coated magnetic stir bar. The flask was immersed in an oil bath heated by a hot plate set at 190 °C. The reactor is open to atmosphere through a trap and a condenser. A small quantity of organics (decane and ketones) as well as water (a condensation product) were collected in the trap after cooled by the condenser operating at 4 °C. Each experiment was conducted for 6-7 h, after which the reactor was cooled down naturally. Reaction mixture was filtered through 0.45-μm PTFE membranes to separate the liquid from the catalysts. Ketone conversion was summarized in **Table S10**. Due to the challenges with separating and identifying the enone products, enone yield and selectivity were not quantified. Instead, the mass yield of "upgradable" condensation products was measured from post-condensation distillation.

Post-Condensation Distillation

The organic phase from the aldol condensation reaction was distilled in a BR Instruments® Micro-distillation column to remove unreacted ketones and solvent. The BR Instruments® Micro-distillation column was run at 50 torr and heated at an initial rate of 12.5% and increased to 17.5% after the first few milliliters of distillate were collected. The reflux ratio was held at 20 until the first few milliliters of distillate were collected at which point the reflux ratio was decreased to 2. The condenser circulating an 80:20 water to ethylene glycol mixture was held at 5 °C for the duration of the distillation. A monel band rotating 120 rpm was used in the column.

Mass Yield and Fraction Composition. The unreacted ketones and solvent fraction (GC trace shown in **Figure S15**) was collected in the distillate from room temperature up to 175°C while the remaining bottoms (enone fraction, GC trace shown in **Figure S16** below) were used for further HDO process. This left approximately 10 wt% of solvent in the fuel which theoretically could be removed but proved difficult in benchtop distillation without significant loss of product. It should also be noted that the unreacted ketones could be removed from the solvent for recycle to the aldol condensation reactor. The mass yield of the enone fraction is 41%. From a carbon content of 73.4% for the ketones and 80.7% for the enones, the C yield of the enone was calculated as 46%.

Hydrodeoxygenation Flow Reactor

Hydrodeoxygenation experiments of ketone and enone sample mixtures were performed in a custom built trickle bed flow reactor consisting of a mass flow controller (Brooks Instruments) for adjusting the flowrate the hydrogen gas, a high-pressure liquid chromatography pump (Chromtech) for controlling liquid addition, a heat-traced inlet line for pre-heating the liquid/gas mixture, a clamshell furnace for temperature control of the reactor tube, a tube-in-tube heat exchanger for condensing liquids from the reactor effluent, and a knock-out pot for collecting liquid product mixtures. A back-pressure regulator (Brooks Instruments) maintained the reactor at a pressure of 500 psig. The liquid and gas feeds mixed above the reactor tube (1/2" outer diameter, Dursan-coated stainless steel (SilcoTek Coating Co.)) and flowed across the Pt/Al_2O_3 catalyst bed (3 wt% Pt, synthesis procedure previously reported. (13) Catalyst bed sizes were increased from our previous work to account for sulfur impurities in the VFA feeds and mitigate deactivation of the platinum sites using previously reported correction factors.(14-16) Liquid samples were analyzed by GC/FID-MS and showed complete conversion with no remaining oxygenate molecules appearing by GC-MS.

Fuel Property Analysis

The fuel properties of the VFA-SAF samples were estimated and measured using Tier α and β respectively. Tier α consists of using GCxGC and GC (17) to conduct hydrocarbon type analysis and distillation curve testing, respectively. The results of this hydrocarbon type analysis is then used to produce property predictions which include density, surface tension, viscosity, cetane number (CN), net heat of combustion (nHOC), flash point, and freeze point. Tier β consists of measuring several key properties, and then using those measurements in combination with correlations to the combustion prediction figure of merit panels to predict likely outcomes of Tier 3 and Tier 4 testing. **Table S2** details the testing volume required and ASTM method for each measurement, alongside properties predicted at each tier. Additional measurements described in the table were taken to supplement typical coverage of the Tier α and β testing.

Sooting Tendency Analysis

Sooting tendency is a fuel property that can be measured at the laboratory scale but is intended to characterize the relative propensity of a fuel to cause soot emissions at the full device scale. In the aviation sector, sooting tendency is typically measured with the ASTM D1322 smoke point (SP) test (18). SP is determined with a specified wick burner and is defined as the height of the test fuel's flame that is at the threshold of emitting soot from its tip. SP is inversely related to sooting tendency: a sootier fuel will produce more soot for a given fuel flowrate and thus soot will break through the tip of the flame at a lower flowrate, which corresponds to a shorter flame. Studies have shown that sooting tendencies derived from 1/SP correlate with emissions from real aviation gas turbines (19).

However, SP has several disadvantages when applied to the development of SAF. First, it requires a relatively large amount of fuel: ASTM D1322 requires 10 mL and recommends 20 mL (18). These volumes are necessary to fully saturate the wick and create a steady-state system, so they cannot be reduced. Second, SP has a narrow dynamic range and cannot be directly applied to fuels whose sooting characteristics differ significantly from Jet A, especially fuels such as SAF that have lower sooting tendencies. The upper limit to the SP that can be measured with the ASTM D1322 apparatus is ~50 mm, which prevents direct measurements for the normal paraffins that dominate the Fast Track VFA-SAF. The SP of n-dodecane, which is near the center of the carbon number distribution for Fast Track VFA-SAF, has been determined by indirect means to be ~60 mm (20).

Therefore, in this study we characterized sooting tendency using a newer approach we have developed that is based on measurements of soot yield in doped methane flames (21). The fundamental concept is to add a small amount of the test fuel (~1000 ppm) to the fuel of a methane/air flame, and then measure the resulting soot concentration. Since the dopant concentration is small, only a small volume of fuel is required (<100 μL per measurement). Furthermore, the dynamic range is large since the method depends on a quantitative soot measurement – instead of the subjective choice of the threshold where soot is emitted from a wick burner flame – and the dopant concentration can be varied to suit different fuels. Indeed, we have successfully applied this approach to hydrocarbons ranging in sooting tendency from methanol (a C1 oxygenated hydrocarbon) to pyrene (a four-ring polycyclic aromatic hydrocarbon) (22). We have shown that the results with this new approach correlate with SP for conventional aviation fuels (23), and independent researchers have reached a similar conclusion (24).

The specific methodology used in the current study was modified to suit SAF. Our earlier work focused on pure hydrocarbons. They were added to the flame at a fixed mole fraction and the resulting soot yield was rescaled into a yield sooting index (YSI) relative to two endpoint compounds with defined values. The current study involves real fuel mixtures, which have a complex composition such that the molecular weight is not know precisely, so they cannot be added to the flame on a mole fraction basis. Instead, they were added at a fixed liquid-phase volumetric flowrate (100 μL/h). Furthermore, the measured soot yields were not rescaled relative to endpoint species but instead they were normalized to the soot yield for the POSF 10325 Jet A sample.

Figure S20 shows the apparatus that was used and previous work(25) describes the specific details of the burner and the diagnostic system. The measurements consisted on three steps: 1) we sequentially doped the Jet A sample and each SAF fuel blend at a uniform liquid flowrate of 100 μL/h into the fuel of a methane/air flame; 2) we measured the maximum soot concentration in each flame with line-of-sight spectral radiance (LSSR); and 3) we normalized the measured LSSR signals into a normalized soot concentration (NSC) for each test fuel defined by Eqn S8 where the subscripts TF, Jet A, and undoped refer to the test fuel, Jet A sample, and the undoped flame. Thus NSC = 1 corresponds to a fuel with the same sooting characteristics as Jet A, and NSC = 0 corresponds to a fuel that produces no soot.

$$\mathrm{NSC} = \frac{\mathrm{LSSR_{TF}} - \mathrm{LSSR_{undoped}}}{\mathrm{LSSR_{Jet\,A}} - \mathrm{LSSR_{undoped}}} \quad (Eqn.S8)$$

The total uncertainty of the reported NSCs is estimated to be ±7%. This includes 1% systematic uncertainty plus 6% random uncertainty. The random uncertainty is based on two standard deviations of six repeated measurements of the 20%/50% Fast Track/Aldol Condensation VFA-SAF blend.

As part of measurement validation, LSSR signals were measured for a series of flames doped with varying flowrates of the 20%/50% Fast Track/Aldol Condensation VFA-SAF blend (**Figure S21**). The results show a strongly linear trend, which indicates that the LSSR diagnostic was operating in a linear regime, and that all of the injected fuel was fully vaporized and reaching the burner.

Techno-economic Analysis

Process model approach. The process model, developed in Aspen Plus, represents a theoretical biorefinery which converts a purified mixture of VFAs to sustainable aviation fuel and naphtha-range fuel. The approach to modeling taken in this work is consistent with that described in prior works (11,

26). Given the uncertainty around emerging technologies and ongoing advancements for the production and separation of VFAs from anaerobic digestion, the decision was made to limit the scope of the process model to a "feedstock" of neat VFAs that can be recovered from fermentation media in their neat, protonated form without salt formation (1-4). However, it should be noted that this commercial VFA-SAF process would likely be coupled with a process for producing VFAs from some low-cost feedstock such as food waste. As such, a feed scale of 26.6 U.S. tons of VFA per day (2.17 MGPY of VFA, associated with the production of 0.94 MGPY of VFA-SAF) of VFAs was chosen for the process. This is based on an assumed food waste plant capacity of 250 wet tons per day (27) with a moisture content of 76.4% (28) and a VFA yield of 0.45 kg/kg dry food waste. Outputs from the model were used to determine equipment sizes and raw material requirements for the process, which were then subsequently used to perform a discounted cash flow rate of return analysis for the construction of a VFA-SAF facility at a commercial scale. High-level process assumptions and results for the TEA are shown in **Table S12-S20**, as well as the overall process block flow diagram (**Figure S17**) and downstream catalytic process flow diagram (**Figure S18**).

The process design builds on prior work relating to the catalytic upgrading of carboxylic acids (11, 29, 30). While these reports have focused on the upgrading of butyric acid, here we have considered a VFA profile with carbon lengths ranging from C_3-C_8 rich in C_4 and C_6 VFAs. This profile, as shown **Table S14**, is based the VFA profile produced from the anaerobic digestion of food waste for a representative feedstock provided by Earth Energy Renewables. For simplicity, isomers of the same carbon length are grouped together and treated as straight-chain VFAs.

Ketonization of mixed VFAs involves binary reactions of all components present. Each reaction involves the formation of a ketone from the carboxylic ends of two VFAs, joining the two molecules and liberating CO_2 and H_2O in the process. Modeled reaction conditions for the VFA upgrading steps are shown in **Table S15** and **S16**. The overall yields of each ketone within the process model were determined using the experimentally validated MATLAB model discussed previously and are shown in **Table S17.** It should be noted here that multiple ketones of any given carbon length would be produced, with the only difference being the location of the ketone group (though it will always be an internal ketone). For simplicity, ketones of the same carbon length are grouped together. Given that the boiling points of these ketones should be very similar, the accuracy of the overall yields of naphtha and SAF fractions should not be affected by this simplification.

VFA ketonization is assumed to take place at 100% conversion with no formation of side products, resulting in a range of ketones in the C_5 to C_{14} carbon length range (the bulk of the ketones are in the C_5 to C_{11} range). The ketone stream exiting the reactor is flashed to remove CO_2; the resulting vapor stream is then scrubbed with water to recover volatile ketones. The liquid bottom product from the scrubber is then decanted to remove the water, yielding a relatively pure stream of mixed ketones. These ketones could potentially be further upgraded into heavier molecules via aldol condensation; however, following the Fast Track process, they are instead routed directly to HDO. In HDO, the ketones are reacted with hydrogen to produce saturated isoparaffins in the jet and naphtha ranges, with oxygen removed from the fuel as water. Unreacted hydrogen from HDO is flashed off and recycled, and the biofuel mixture is sent to an additional distillation column for fractionation into naphtha and jet range blendstocks. Utility requirements for the process, including grid electricity, cooling water, steam, hot oil, and storage are accounted for the model. Steam and hot oil requirements for the process are met by with natural gas, with process off-gases also utilized. Off-site wastewater treatment costs are calculated on a chemical oxygen demand (COD) basis using a $/kg COD cost factor from literature (26).

The engineering approach taken in this work is similar to that described in prior reports and will not repeated in the same detail here (11, 26). The overall mass energy balance from the Aspen Plus model was used to determine the number and size of capital equipment items needed. As process conditions and flows change, baseline equipment costs are automatically adjusted in an Excel spreadsheet using scaling factors. These baseline costs come from vendor quotes when available and are estimated in Aspen Capital Cost Estimator (ACCE) when necessary. The details of these equipment designs have been published in prior reports (11, 31).

Once equipment costs are determined, direct and indirect overhead cost factors are applied to determine a feasibility-level estimate of total capital investment (TCI) in 2016 dollars. These factors are shown in **Table S18** along with purchased and installed equipment costs for each area. Operating expenses are based on raw material and utility rates from the Aspen Plus model and are shown in **Table S19**; fixed

costs are based on prior works and adjusted based on plant scale and are shown in **Table S20.** The TCI, operating expenses, and fixed costs are used in a discounted cash flow rate of return analysis. Prior analyses typically use this discounted cash flow analysis to determine a minimum fuel selling price (MFSP) required to obtain a net present value (NPV) of zero for the plant. In this analysis, the fuel price is instead set to an assumed market value, in $/gallon gasoline equivalent (GGE), and a target production cost of VFA (termed "VFA production cost") is determined that will result in an NPV of zero. This alternate strategy allows for a clear identification of target production costs for potential upstream VFA production and separation processes. Financial assumptions used in this analysis are shown in **Table S13**, which are based on a mature n^{th} plant and consistent with prior published work.

Plant scale can be seen to have a large impact on production cost of VFAs price due to the economy of scale effect; however, it is not directly related to the VFA upgrading operation and is thus reported separately. In this analysis, the plant scale is limited by the availability of the original upstream feedstock (assumed here to be food waste) which is converted to VFAs. Centralized processing facilities are a concept often applied to biorefineries for the purpose of achieving increased scaling efficiencies by processing biomass from a wider area through one facility. Food waste, at an asserted scale of 250 wet tons per day, could potentially be collected and sent to a centralized facility for VFA production and upgrading. This would result in equipment savings for both VFA production and upgrading processes at the increased scale. However, it would also likely incur significant shipping costs in centralizing the food waste. Alternatively, it might make more sense to allow for VFA production facilities to stay at the smaller, local scale, and send VFA product streams to a centralized facility dedicated to upgrading. Shipping costs would be much lower vs. a centralized food waste facility, with VFA shipping needs equating to only 10% of the shipping needs for wet food waste by mass. A more comprehensive analysis would need to be done to determine exactly what kind of scale benefits would be possible from a centralized facility. Given this uncertainty, a range of plant scales were considered; the relationship between a plant scale and the VFA production price is shown in **Figure S19**.

Life Cycle Analysis

The life cycle modeling boundary for this study is from feedstock to the use of finished product, including upstream emissions and embodied energy associated with the inputs used in the fuel conversion processes. The functional unit is 1 MJ of jet fuel in aviation jet application. When the conversion processes (e.g., the VFA production facilities, petroleum refineries) produce more than one energy product (e.g., jet fuel, naphtha), an energy-based approach is applied to allocate emissions among products. Material and energy flow data used for modeling the life cycle carbon intensity of VFA-SAF is informed by the ASPEN process model inputs and output along with upstream data derived from GREET, SimaPro, and literature (as summarized in **Table S21-S22**). Combustion CO_2 emissions per MJ of VFA-SAF were calculated based on the carbon content of the biofuel. Consistent with LCA convention (32), a carbon credit is provided to CO_2 emissions from the combustion of VFA-SAF that assumes food waste is 100% biomass-based. Any percentage of non-biogenic carbon fed into the process would impact both the upstream and downstream emissions, and was outside the scope of this work. As discussed in the main text, the waste management practice currently used for food waste may evolve in the future, which would significantly influence the emissions credit allocated to diverting food waste from landfill. LCA results can vary considerably, depending on the assumptions employed, baseline defined (e.g., current food waste management practice), co-product allocation method, among others. For comparison, the carbon intensity for the fossil-based U.S. average ultra-low sulfur jet fuel is derived from the GREET model (GREET_1 2019). The goal of this analysis is to highlight the potential upper bound of GHG reductions for VFA-SAF based on current LCA practices and technology performance parameters outlined here, as well as highlight the dependencies on emission credits to guide future research and development efforts for further GHG reductions.

Section S2: Supplementary Data

Table S1. Comparison of current ASTM 7566 routes for SAF. These conversion pathways and their fuel properties are covered in further detail in recent reviews (33).

ASTM-approved SAF pathway	Description and Considerations
Fischer-Tropsch synthesized paraffinic kerosene (SPK) Municipal solid waste, agriculture and forestry waste Annex 1. Approved 50% blend	Gasification of dry waste and lignocellulosic feedstocks. Normal and isoparaffin fuel. Capital for constructing Fischer-Tropsch processing plants major consideration.
HEFA-SPK Vegetable oil, waste fats, oils, waste grease Annex 2. Approved 50% blend	Hydrotreating vegetable oils, as well as waste fats, oils, and greases. Normal and isoparaffin fuel. Waste lipid feedstock availability major consideration.
Synthesized Iso-Paraffins (SIP) Farnesane Annex 3. Approved 50% blend.	Biological fermentation of sugar to farnesene, followed by catalytic hydrogenation to farnesane. Isoparaffin fuel comprised predominantly of farnesane. Source of sugar major consideration.
Fischer-Tropsch synthetic kerosene with aromatics (SKA) Municipal solid waste, agriculture and forestry waste Annex 4. Approved 10% blend	Targets gasification of dry waste and lignocellulosic feedstocks. Tailor process to produce aromatics. Similar considerations as Fischer-Tropsch SPK above, with lower blend limit of 10%.
Alcohol-to-Jet SPK Ethanol or isobutanol Annex 5. Approved 30% blend	Fermentation of sugars to ethanol or isobutanol; waste gas fermentation to ethanol. Normal and isoparaffin fuel. Source of feedstock major consideration for carbon intensity.
ARA Catalytic Hydrothermolysis Jet (CHJ) Waste fats, oils, and grease Annex 6. Approved 50% Blend	Hydrothermally processed fatty acid esters and fatty acids. Fuel includes n-paraffins, iso-paraffins, and aromatics. Waste lipid feedstock availability major consideration.
IHI Hydrocarbon (HC)-HEFA Botryococcenes Annex 7. Approved 10% Blend	Hydrocarbons, esters and fatty acids produced from *Botryococcus braunii*. Cost and scalability of algal hydrocarbons main consideration.

Table S2. Volume required and method for measuring associated properties for Tier α, Tier β, and additional measurements

Evaluation Category	Measured Property	Predicted Property	Test Volume
Tier α	Hydrocarbon Type Analysis (GCxGC)	nHOC, Density, Surface tension, Freeze point, Viscosity, DCN, Flash point	~1 mL
	Simulated Distillation (ASTM D2887)		
Tier β	Density (ASTM D4052)	nHOC	~10 mL
	Viscosity (ASTM D7042)		
	Surface tension (ASTM D1331A)		
	Freeze point (ASTM D5972)		
	Flash point (ASTM D3828A)		
	ICN (ASTM D8183)**		~40 mL (140 mL with conventional DCN ASTM D6890)
Additional Measurements	Net Heat of Combustion (D240 calculation)	-	-
	HOC (ASTM D4809)		~6 mL
	%H (LECO CHN 628 elemental analyzer)		~0.6 mL
	Acid Content (ASTM D664)**		~5 mL
	Nitrogen Quant. (ASTM D4629)		~5 mL
	Yield sooting index (published method(23))		~0.5 mL

* Not in ASTM screening requirements
** Alternative method to that listed in ASTM D7566 Table 1 or ASTM D1655 Table 1

Table S3. Biogenic VFA distributions (mol%, dry basis) that were prepared as feedstocks for ketonization reactions. These same distributions were used for ketonization model calculations.

Sample	C_2	C_3	C_4	i-C_4	C_5	i-C_5	C_6	C_7	C_8
C_4	0.8	15.9	64.5	2.5	11.3	3.5	1.5	0.0	0.0
C_4/C_6	0.5	13.3	53.9	2.1	9.4	2.4	17.7	0.0	0.0
C_6/C_8	0.0	1.6	14.3	0.1	5.1	0.6	49.7	0.9	27.7

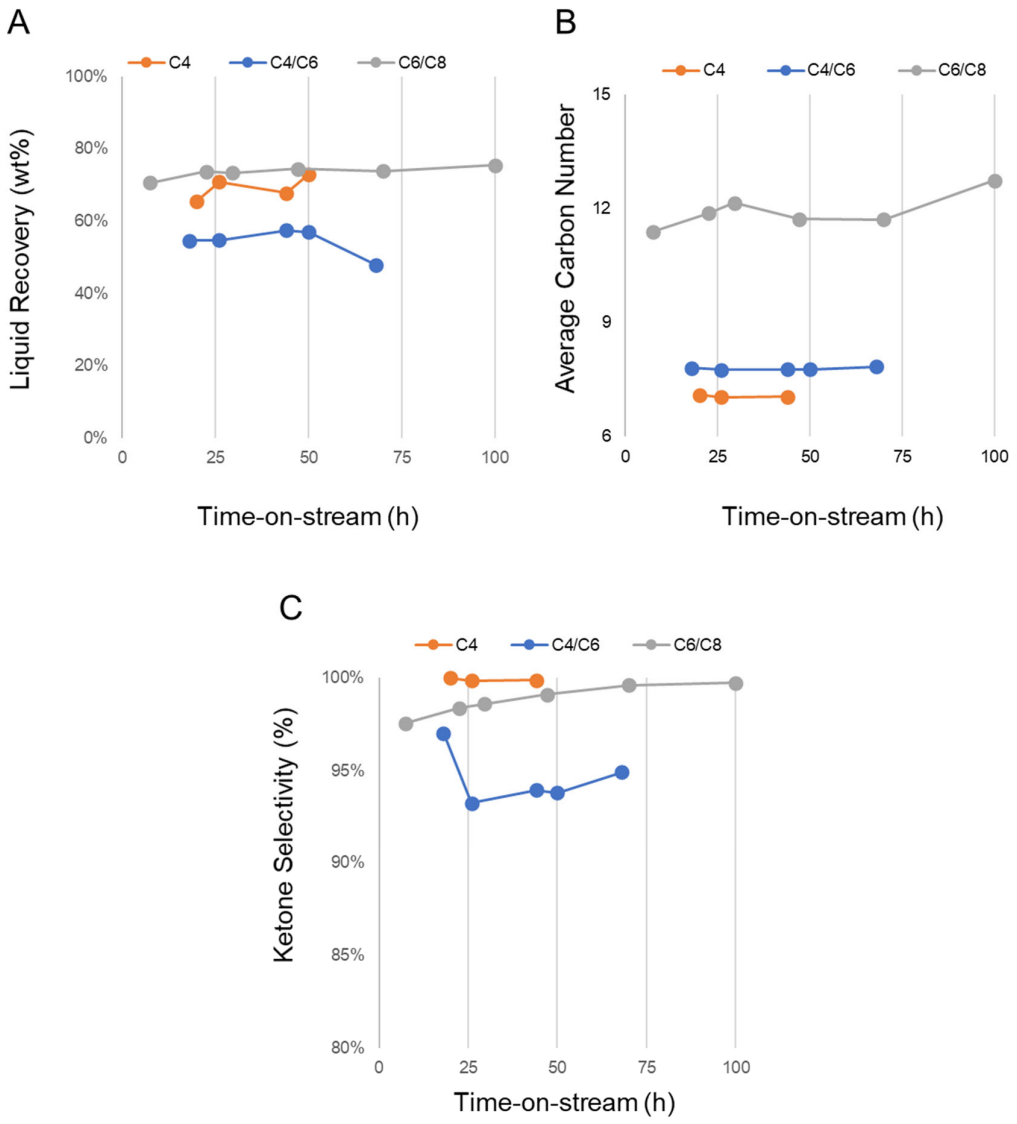

Figure S1. Time-on-stream variation during ketonization for the various VFA samples. Parameters tracked include: (A) liquid mass recovery, which includes both the organic ketone phase and aqueous phase fractions, (B) average ketone product carbon number, and (C) selectivity to ketones.

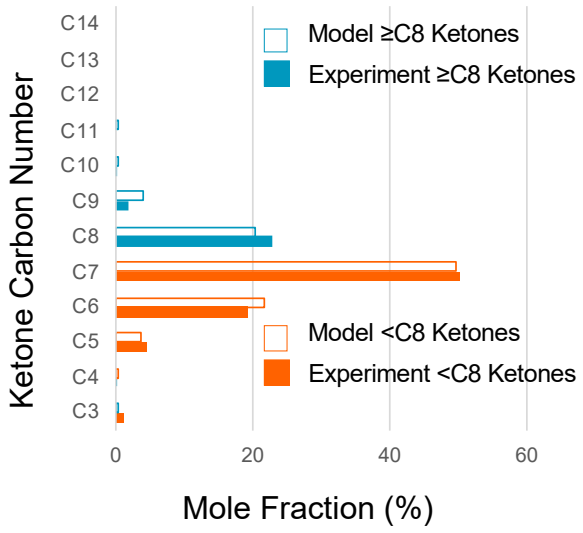

Figure S2. Modeled and experimental VFA ketonization carbon yields for C_4 VFA feed. Blue represents $\geq C_8$ ketone carbon chain lengths suitable for Fast Track VFA-SAF, while orange represents $\leq C_7$ ketones that require coupling for Aldol Condensation VFA-SAF.

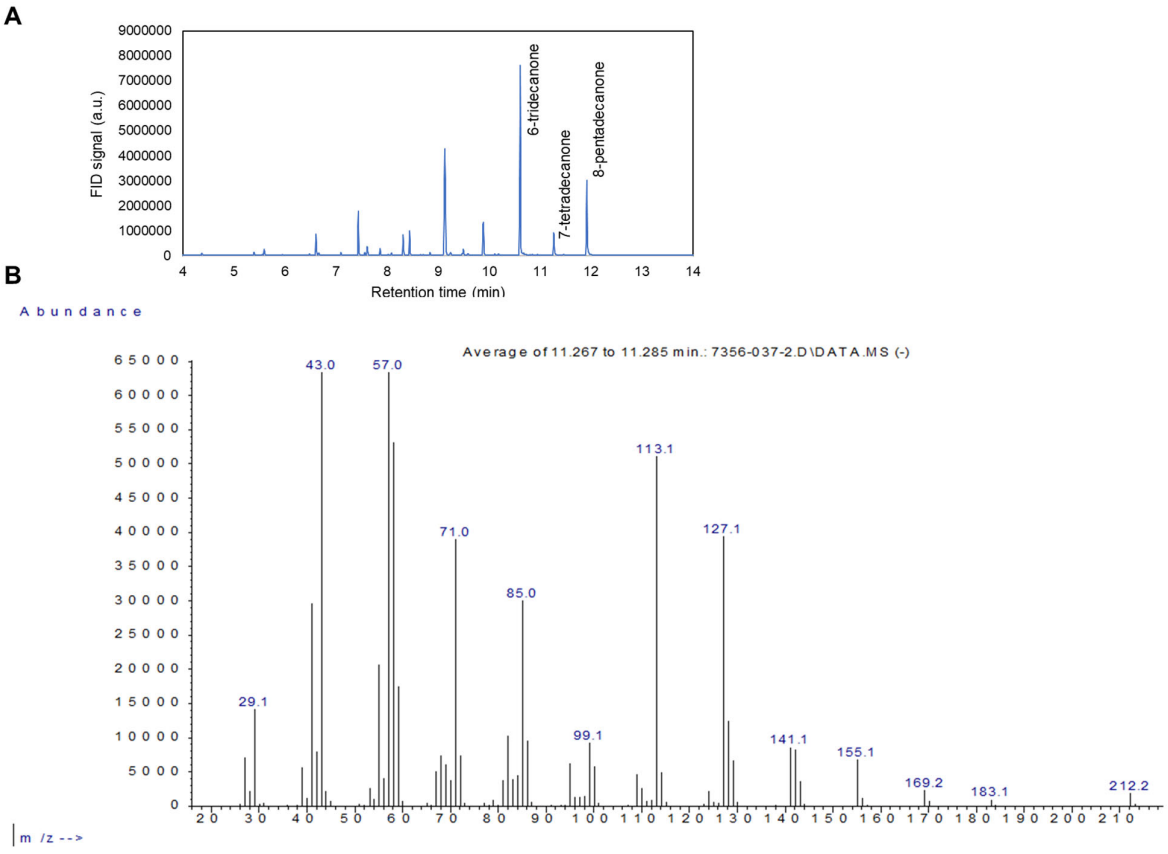

Figure S3. GC analysis of the VFA ketonization liquid product mixture for the C_6/C_8 VFA feed. (A) GC trace and (B)MS fragmentation pattern for the peak eluting at 11.27 min assumed to be 7-tetradecanone based upon the parent ion mass of 212.2 m/z.

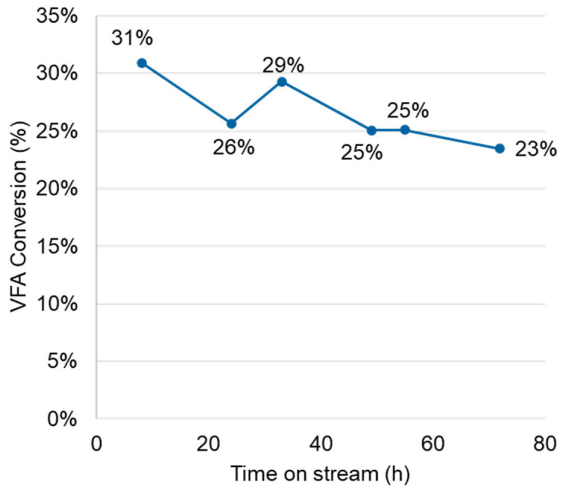

Figure S4. Ketonization catalyst stability under partial conversion conditions for 72 h of time-on-stream using model VFA's (Sigma-Aldrich) with a distribution to simulate the C_4/C_6 stream. Reaction conditions: Catalyst loading 2 g ZrO_2, Ar flow 166 mL (STP) min^{-1} at 1 atm, bed temperature 290 °C, WHSV 7.7 h^{-1} based on VFA mass flow rate.

Table S4. Surface composition (atomic%) of fresh, spent, and regenerated ZrO_2 determined by XPS.

Catalyst	Zr	O	C	Na
Fresh	18.1	45.4	36.3	0.3
Spent	13.1	36.0	50.4	0.5
Regen	17.5	12.7	37.9	0.3

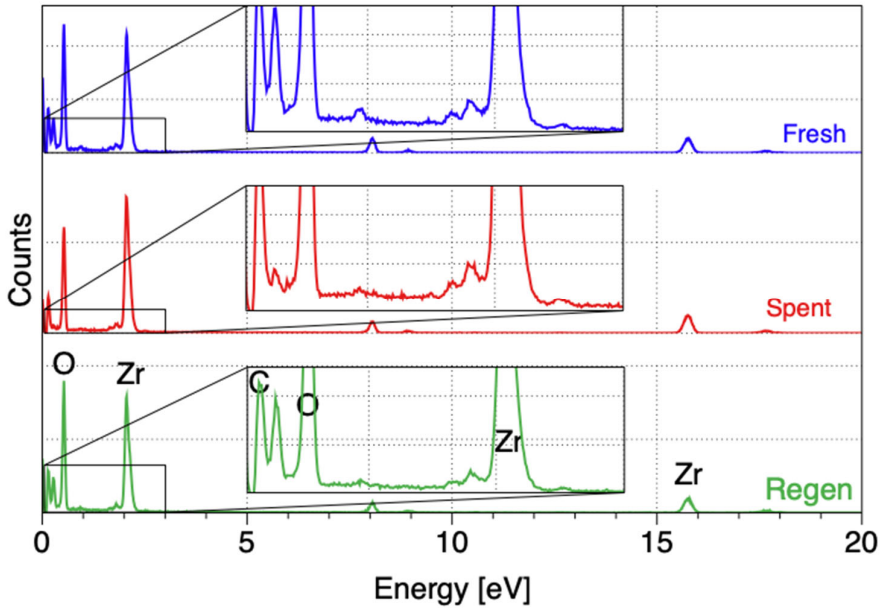

Figure S5. EDS spectra generated from fresh, spent, and regenerated ZrO_2.

Table S5. Elemental analysis of the aqueous phase product of C_6/C_8 food-waste derived VFA ketonization.

ppm	C_6/C_8 Ketonization Aqueous Product
Al	<1
B	2
Ca	2.0
Fe	<1
K	<1
Mg	0.2
Mn	<0.2
N	ND
Na	26
P	<10
S	<10
Si	4
Zn	<1
ND: Not determined due to volume limitations	

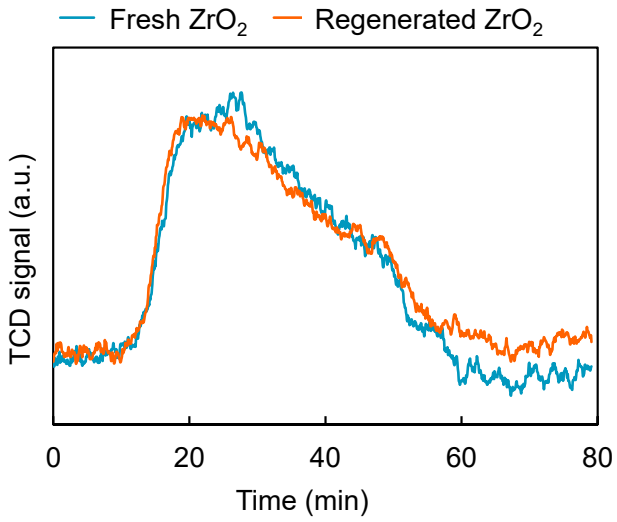

Figure S6. Comparison of NH_3 desorption profile between fresh ZrO_2 catalyst and regenerated ZrO_2 catalyst.

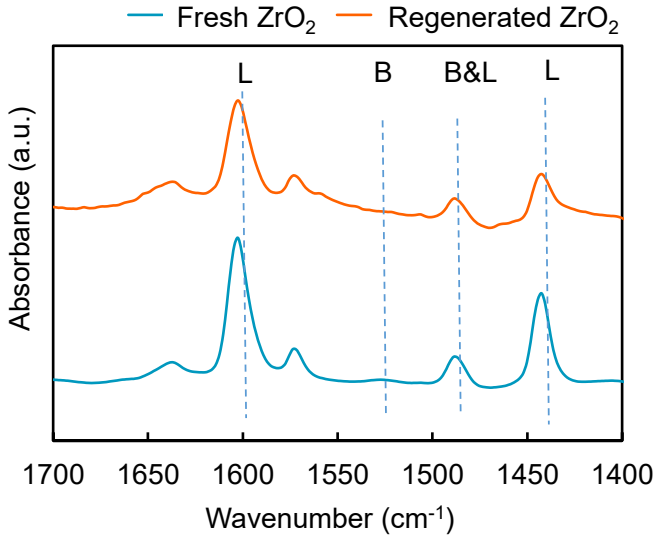

Figure S7. DRIFT spectra of pyridine adsorption on fresh ZrO_2 catalyst and regenerated ZrO_2 catalyst.

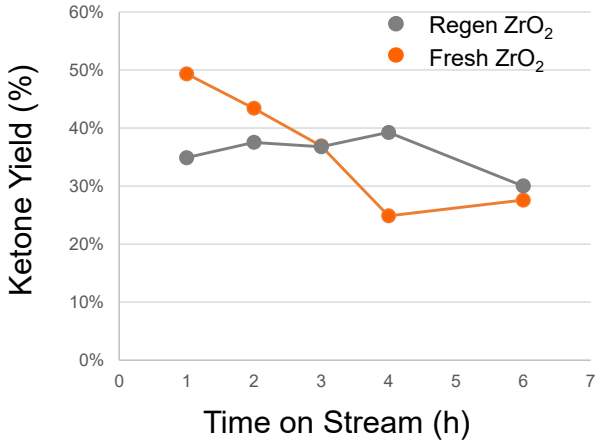

Figure S8. Liquid product analysis of ketonization catalyst testing under partial conversion conditions before and after regeneration using the spent full conversion catalyst. Reaction conditions: Catalyst loading 2 g ZrO_2, Ar flow 166 mL (STP) min^{-1} at 1 atm, bed temperature 290 °C, WHSV 7.7 h^{-1} based on VFA mass flow rate. Catalyst regeneration conditions: 5 °C/min to 500 °C, hold 12 h, cool naturally, in flowing air.

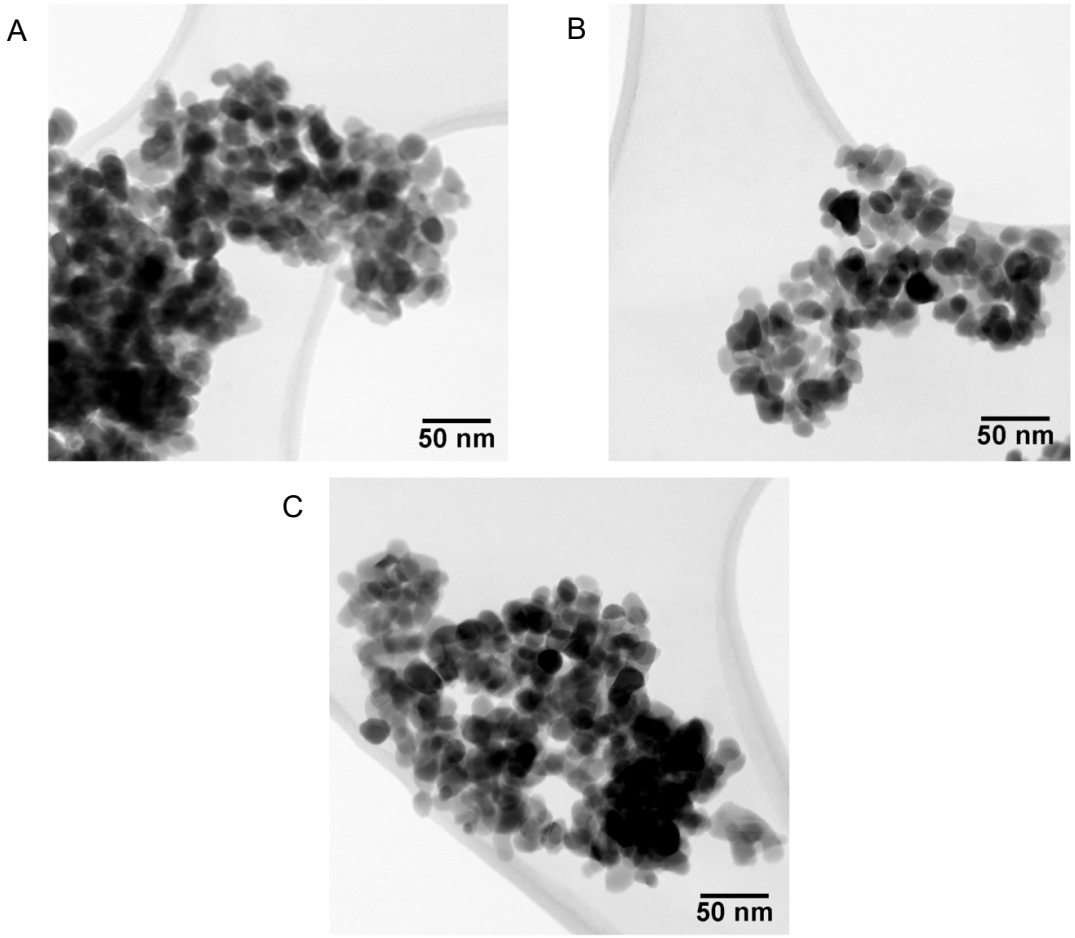

Figure S9. Bright field (BF) STEM images of the ZrO_2 catalyst used for VFA ketonization. Images include the (A) fresh catalyst, (B) spent 100-h sample used for processing the food waste-derived C_6/C_8 VFA sample, and (C) regenerated ZrO_2.

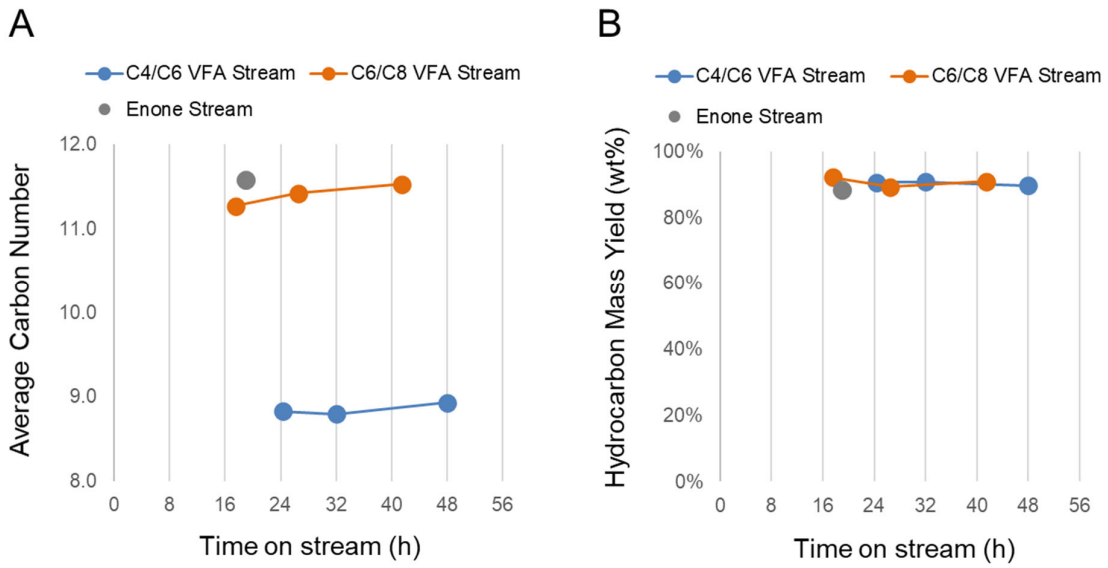

Figure S10. Time-on-stream variation during ketone and enone hydrodeoxygenation for various samples. Properties tracked include (A) average hydrocarbon carbon number and (B) hydrocarbon mass yield.

Table S6. Typical commercial Jet A carbon number distribution (>0.1 mass%, 11.4 carbon average) as shown in gray shading of main text **Fig. 4A**, **D**, and **G**.

Sample	C_5	C_6	C_7	C_8	C_9	C_{10}	C_{11}	C_{12}	C_{13}	C_{14}	C_{15}	C_{16}	C_{17}	C_{18}
Jet A	0	0.57	2.06	5.98	12.93	19.29	17.92	16.63	10.64	7.73	3.83	1.54	0.48	0.14

Table S7. Net heat of combustion of commercial Jet A in comparison to VFA-SAF and currently approved ASTM SAF routes.

SAF Sample	POSF	Average Formula	ASTM D7566 Annex	nHOC, MJ/kg
Commercial Jet A	10325	$C_{11.4}H_{22.0}$	N/A	43.0
C_6/C_8 Fast Track VFA-SAF	N/A	$C_{10.8}H_{23.6}$	N/A	43.4
C_4/C_6 Fast Track VFA-SAF	N/A	$C_{9.1}H_{20.0}$	N/A	44.5
C_4/C_6 Aldol Condensation VFA-SAF	N/A	$C_{13.5}H_{28.8}$	N/A	44.1
2/5 Blend Ratio C_4/C_6 Fast and Aldol Cond. VFA-SAF	N/A	$C_{12.4}H_{25.0}$	N/A	43.7
Syntroleum Fischer Tropsch SPK	5018	$C_{11.8}H_{25.6}$	A1	44.1
Dynamic Fuels HEFA SPK	7272	$C_{12.4}H_{26.7}$	A2	43.9
Sasol Fischer Tropsch SPK	7629	$C_{10.8}H_{23.4}$	A1	43.7
UOP HEFA SPK	10301	$C_{12.0}H_{25.9}$	A2	43.9
Gevo Alcohol-to-Jet	11498	$C_{12.6}H_{27.2}$	A5	43.9
Lanzatech Ethanol-to-Jet	12756	$C_{11.7}H_{25.4}$	A5	43.9

Table S8. Fuel properties for n-paraffin Fast Track VFA-SAF and isoparaffin Aldol Condensation VFA-SAF, alongside blend criteria and Jet A fuel properties.

Property	10% SAF Jet Blend Criteria[a]	Jet A	Fast Track C_6/C_8 VFA-SAF			Fast Track C_4/C_6 VFA-SAF			Aldol Cond. C_4/C_6 VFA-SAF		70% Co-Blending VFA-SAF Fast Track/Aldol Cond. [d]
			10%	20%	100%	10%	20%	100%	30%	100%	
$T_{cloud\ or\ freeze}$ (°C)	*< -40*	-52	-47	-44.5	-26.9	-50.9	-52.2	-61.7	-52.6	-53.4	-60.7
IBP (°C)[b]	-	159	151	148	102	150	140	136	151	181	143
T5 (°C)	-	173	169	164	135	165	162	142	179	209	165
T10 (°C)	*Ph. < 205*	177	175	174	147	171	162	138	184	216	173
T20 (°C)	-	185	185	183	166	178	172	147	193	218	189
T30 (°C)	-	192	191	192	176	186	178	146	200	220	198
T50 (°C)	*report*	205	206	206	199	202	195	149	212	222	213
T70 (°C)	-	221	220	221	219	218	214	153	224	228	223
T80 (°C)	-	231	229	230	223	228	225	165	233	242	233
T90 (°C)	*report*	245	243	243	235	242	240	179	251	268	254
T95 (°C)	-	256	255	254	256	254	254	183	268	290	277
T_{boil} or T100 (°C)	*Ph. < 300*	271	270	268	271	267	267	202	289	309	298
Density, 15 °C (g/mL)	*0.775-0.840*	0.802	0.798	0.792	0.743	0.795	0.787	0.723	0.796	0.780	0.776
ν, 15°C (cSt)		1.8	ND	ND	ND	1.81	1.70	1.07	2.14	2.78	1.96
ν, - 20°C (cSt)	*< 8*	4.7	4.38	4.30	3.45	4.02	3.64	1.91	5.23	8.38	4.62
ν, - 40°C (cSt)	*< 12*	9.551	8.89	8.64	-	7.95	6.96	2.99	11.54	24.17	9.97
Surface Tension, RT (mN/m)	-	24.8	25.8	25.1	24.0	25.8	25.0	23.1	25.8	25	24.2
T_{flash} (°C)	*38-66 (or ≥38)*	48	48	>38	31	42	39	24	53	62	39
%C	-	86.1	86.3%	85.5%	84.3%	85.7%	85.7%	83.0%	85.2%	84.9%	84.7%
%O	-	0	0.7%	0.6%	0.7%	0.7%	0.4%	2.4%	1.2%	0.4%	1.2%
%H	-	14%	14.4%	13.9%	15.4%	13.6%	13.8%	14.6%	13.6%	14.7%	14.2%
N (mg/kg)	< 2	ND	ND	ND	ND	ND	ND	<1.0	1.2	ND	ND
Acidity (mg KOH/g)	-	0.005	ND	ND	ND	ND	ND	0.15	0.10	ND	ND
nHOC (MJ/kg)	*> 42.8*	43.01	43.18	43.43	43.98	43.39	43.39	44.49	43.45	44.41	43.74
LHV (MJ/L)	*≥Jet A**	34.49	34.45	34.40	32.68	34.50	34.15	32.18	34.59	34.62	33.93
Cetane Number (CN)	-	48.4	51.5	53.0	ND	50.9	51.9	63.6	*56*	*73*	63.6
NSC[c]	*≤ 1**	1	*0.94*	0.87	*0.35*	0.93	0.87	0.35	0.85	0.53	0.66

*Criterion not part of ASTM

Italics: Predicted derived cetane number using Tier α evaluation

a Blend criteria for 10 vol% SAF in commercial jet fuel primarily from ASTM D7566 Table 1 or ASTM D1655 Table 1. Red text indicates value outside of this specification.

b Ph. Indicates physical distillation; otherwise, assume simulated distillation criteria or measurements

c Normalized soot concentration (Jet A = 1) using yield sooting index method

d 20% Fast Track C_4/C_6 VFA-SAF with 50% Aldol Cond. C_4/C_6 VFA-SAF in Jet A

Table S9. Flashpoint (°C) of the Fast Track C_6/C_8 VFA-SAF, Fast Track C_4/C_6 VFA-SAF, and Aldol Condensation C_4/C_6 VFA SAF, with out-of-specification (flashpoint < 38 °C) in red.

SAF Blend	Fast Track C_6/C_8 VFA-SAF	Fast Track C_4/C_6 VFA-SAF	Aldol Cond. C_4/C_6 VFA-SAF
10%	48	42	-
20%	38	39	-
30%	-	-	53
50%	34	-	-
100%	31	24	62

Table S10. Percent conversion $([R_{in}] - [R_{out}])/[R_{in}]$ of mixed ketone aldol condensation.

Component	Trial 1	Trial 2	Trial 3	Average
2-pentanone	100%	100%	100%	100%
3-pentanone	92%	92%	93%	92%
3-hexanone	77%	76%	76%	76%
2-methyl-3-hexanone	41%	40%	32%	38%
4-heptanone	58%	58%	55%	57%
3-heptanone	61%	65%	61%	63%
2-methyl-4-heptanone	32%	34%	29%	32%
3-Methyl-4-heptanone	14%	16%	7%	12%
5-dimethyl-3-hexanone	22%	29%	13%	21%
4-octanone	52%	53%	48%	51%
3-octanone	70%	73%	71%	71%
4-nonanone	49%	50%	44%	48%
decane (solvent)	-2%	-4%	-3%	-3%

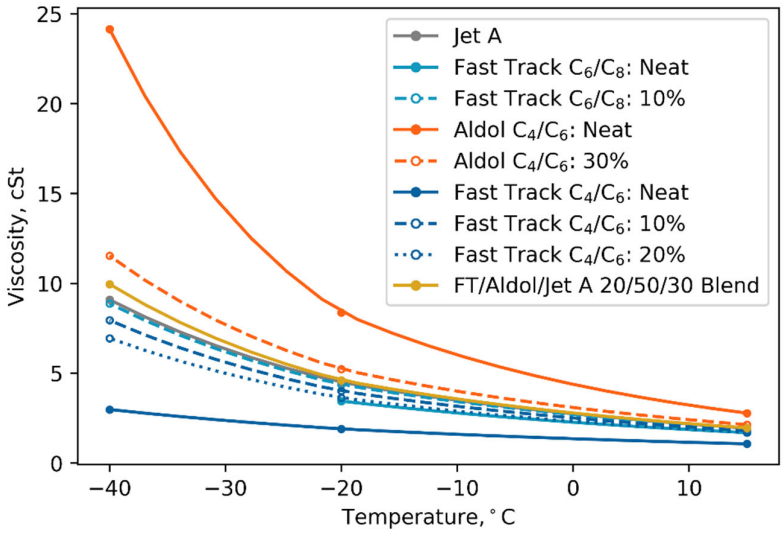

Figure S11. Viscosity as a function of temperature for the Fast Track C_6/C_8 VFA-SAF, Fast Track C_4/C_6 VFA-SAF, Aldol Condensation C_4/C_6 VFA-SAF, and Co-Blending (Fast Track/Aldol Cond. mixture) C_4/C_6 VFA-SAF.

Table S11. Diesel fuel properties of the Aldol condensation C4/C6 VFA fuel, ultra-low sulfur diesel fuel (ULSD), and HEFA diesel (34) compared against the diesel bioblendstock fuel screening criteria established by the Co-Optimization of Fuels & Engine (Co-Optima) project sponsored by the Department of Energy (35). Similar advantaged diesel fuel properties were established when processing butyric acid from fermentation through the aldol condensation pathway, as described in our earlier work (13).

Diesel Fuel Property	**Diesel Bioblendstock Criterion**	**Ultra-low Sulfur Diesel**	**HEFA Diesel A**	**Aldol Cond. C_4/C_6 VFA Biofuel**
Cloud point (°C)	<0	-28	-27	-53
Boiling point/T90 (°C)	<338	300	287	268
Flash point (°C)	≥52	73	65	62
Density at 15°C (g/mL)	NA	0.847	0.775	0.780
Kin. Viscosity at 40°C (cSt)	NA	2.5	2.5	ND
LHV (MJ/kg)	NA	42.88	44.45	44.41
Cetane number	≥40	48	74	73
NSC (Jet A = 1)	NA	1.08	ND	0.53
Water solubility (mg/L)	< 20 g/L	insoluble	insoluble	insoluble

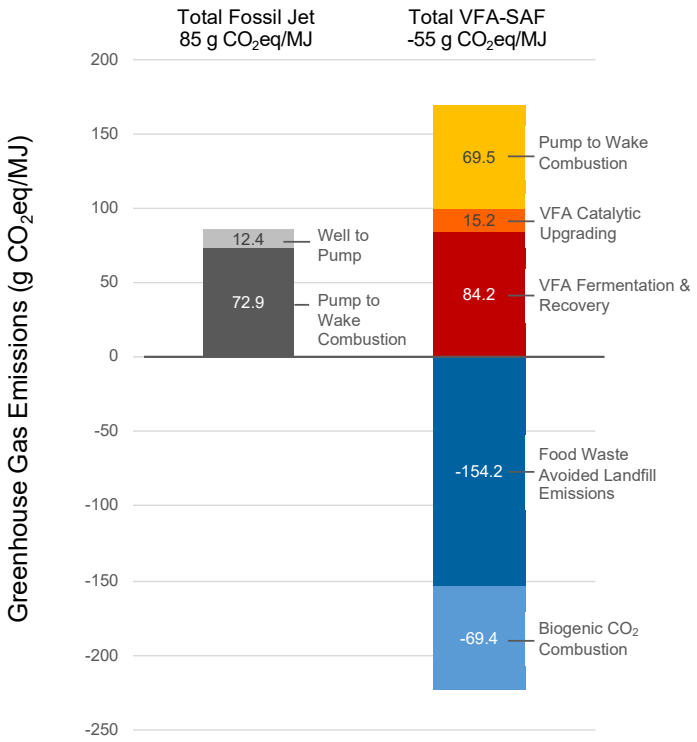

Figure S12. GHG contributions for Fast Track VFA-SAF derived from food waste relative to fossil jet. For fossil jet, "Pump to Wake" combustion accounts for emissions from burning fossil fuel. Combustion of VFA-SAF would also result in GHG emissions of 69.5 gCO_2eq/MJ based on the carbon content of the fuel (69.4 gCO_2/MJ), which is slightly higher than conventional fossil jet fuel, and CH_4 and N_2O emissions (0.1 gCO_2eq/MJ). For this analysis, we assume VFA-SAF is comprised of biomass carbon, which would receive an equivalent biogenic CO_2 credit to offset its combustion. In addition, VFA-SAF produced with food waste diverted from landfills would receive an additional CO_2 credit due to avoided landfill emissions that include mainly methane. As discussed in the main text, food waste management practices may evolve in the future, which could significantly influence or eliminate the credit allocated to diverting food waste from landfills. The largest source of GHG emissions with VFA-SAF is due to VFA fermentation and recovery, which is an emerging technology area under active development. Resource consumption, waste streams, and utilities are anticipated to vary based on the upstream process technology configuration, waste feedstock composition, technology readiness level, and scale of implementation. See **Table S17** for additional upstream details. VFA catalytic upgrading emissions were based on the "Fast Track" process modeling described within this scope of work. See **Table S18** for additional downstream details. When accounting for the credits and emissions listed here, VFA-SAF life cycle GHG emissions are -55 gCO_2eq/MJ, which is 165% lower than fossil jet fuel. If the credit associated with avoided food waste landfill emissions is not included, the life cycle GHG emission for VFA-SAF would increase to 99 g CO_2eq/MJ, which is 16% higher than fossil jet fuel. Given the emerging stage of VFA-SAF technology, these results emphasize the need to account for wet waste feedstock selection and current disposal management practices, as well as further reduce the GHG emissions associated with VFA-SAF conversion technology.

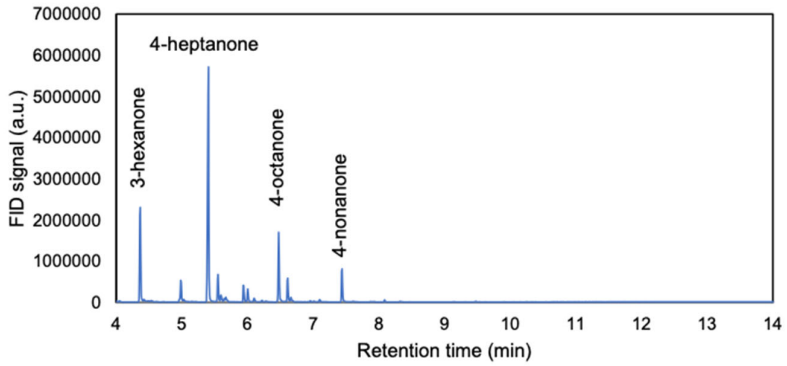

Figure S13. GC trace of the lighter (predominantly $\leq C_7$) ketones after distillation.

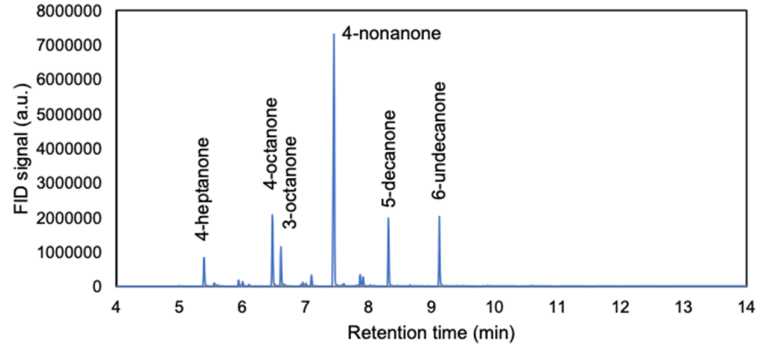

Figure S14. GC trace of the heavier (predominantly $\geq C_8$) ketones after distillation.

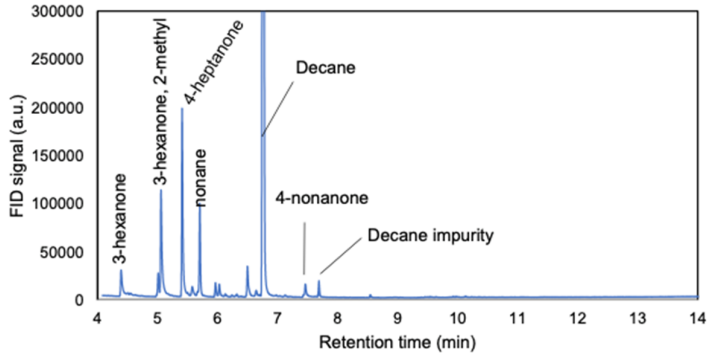

Figure S15. GC trace of the unreacted ketones from aldol condensation and the solvent fraction.

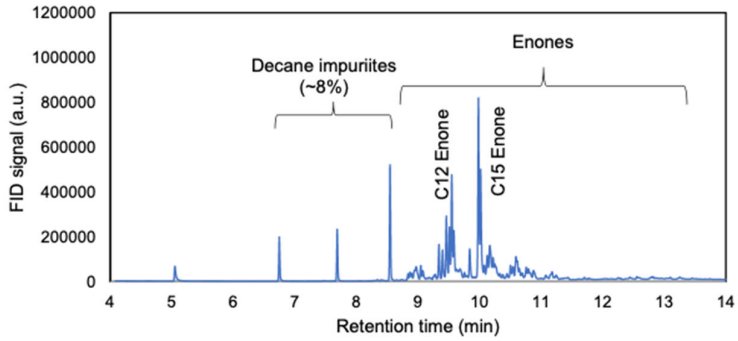

Figure S16. GC trace of the enone fraction following ketone aldol condensation and distillation.

Table S12. Key process assumptions for the baseline downstream VFA catalytic upgrading TEA model for a representative plant processing 250 wet U.S. tons of food waste per day. 1 GGE = 122.5 MJ/gal; 1gallon jet equivalent (GJE) =130.4 MJ/gal.

VFA Production (for determining VFA upgrading scale only)	
Plant Scale	250 wet US. tons food waste/day
VFA yield	0.45 kg/kg dry food waste
Food waste moisture content	76.4%
VFA Catalytic Upgrading	
Downstream Plant Scale	26.6 U.S. tons per day 6600 gal VFA per day 2.17 MGPY VFA
On stream factor	90%
Fuel selling price	$2.50/GGE
Maximum VFA production cost	$1.08/gal of VFA $0.30/kg of VFA
Carbon efficiency (VFA to liquid fuel)[a]	84.7% (45.8%)
Total fuel production (MGPY GGE basis)[a]	1.63 (0.88)
Total VFA-SAF production (MGPY GJE basis)	0.94
Total fuel yield (GGE/gallon VFA)[a]	75.1% (40.6%)

[a] Number in parenthesis indicates value for SAF only, with remainder attributed to naphtha

Table S13. Financial assumptions and design basis used for the VFA catalytic upgrading TEA model.

Financial Assumptions	
Plant life	30 years
Plant throughput	1004 kg/hr of VFA
Cost year dollar	2016$s
On-stream factor	90%
Discount rate	10%
General plant depreciation	MACR
General plant recovery period	7 years
Steam plant depreciation	MACR
Steam plant recovery period	20 years
Federal tax rate	21%
Financing	40% equity
Loan terms	10-year loan at 8% APR
Construction period	3 years
First 12 months' expenditures	8%
Next 12 months' expenditures	60%
Last 12 months' expenditures	32%
Working capital	5% of fixed capital investment
Start-up time	6 months
Revenues during start-up	50%
Variable costs during start-up	75%

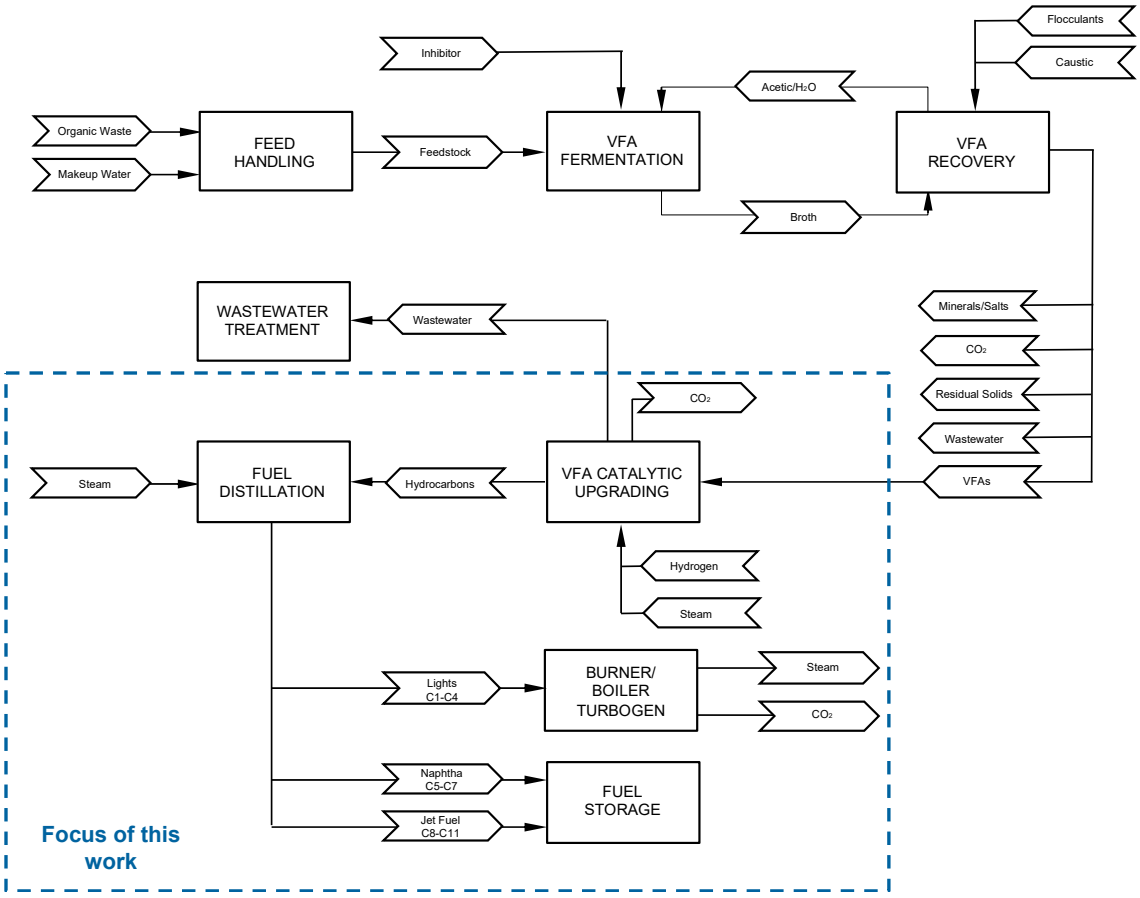

Figure S17. High level block flow diagram showing key process areas of the TEA model. Representative VFA fermentation and recovery process inputs and outputs were based on technical consultation with Earth Energy Renewables for this early-stage technology. As noted, VFA fermentation and recovery is an emerging technology area under active development, with process flow streams anticipated to vary based on the upstream process technology configuration, waste feedstock composition, technology readiness level, and scale of implementation. The scope of this work focuses on downstream VFA catalytic upgrading.

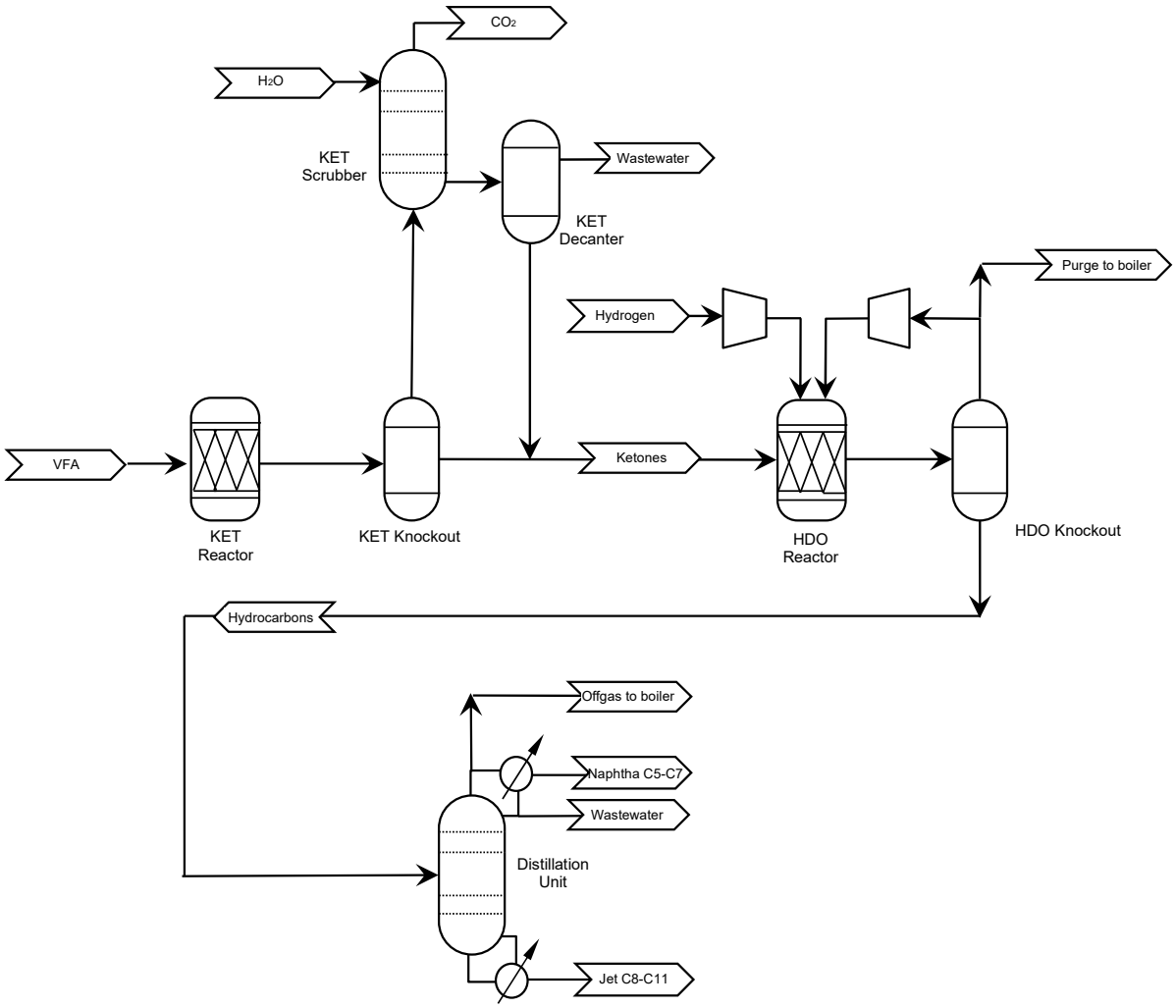

Figure S18. Process flow diagram for VFA catalytic upgrading unit operations employed for the "Fast Track" process. Heat exchangers are omitted for simplicity.

Table S14. Modeled VFA profile used in the downstream catalytic upgrading Aspen model for the TEA, based on inputs from industry partner Earth Energy Renewables for a representative food waste fermentation run that produces a C_4/C_6-rich profile. As noted, VFA fermentation and recovery is an emerging technology area under active development and VFA profiles are highly dependent on food waste nutritional composition, fermentation parameters, and separation technology.

VFA Carbon Length	Mole Percent	Weight Percent
C_3	13.0	10.4
C_4	57.7	54.8
C_5	12.7	14
C_6	16.3	20.4
C_7	0.2	0.3
C_8	0.1	0.1

Table S15. Summary of key process parameters in the catalytic upgrading portion of the TEA model.

Ketonization	
Temperature	365°C
Pressure	1 atm
Catalyst	ZrO_2
WHSV	6 h^{-1}
Hydrodeoxygenation	
Temperature	270-320°C
Pressure	500 psig
Catalyst	3% Pt/Al_2O_3
WHSV	3 h^{-1}

Table S16. Summary of reaction stoichiometry for catalytic upgrading steps.

Reaction	Stoichiometry
Ketonization	2 Carboxylic Acid → Ketone + CO_2 + H_2O
Hydrodeoxygenation	Ketone + 2 H_2 → Hydrocarbon + H_2O

Table S17. Modeled ketone profile for the downstream VFA catalytic upgrading TEA, with values based on outputs of the kinetic MATLAB model.

Ketone Carbon Length	Mole Percent	Weight Percent
C_5	1.7	1.2
C_6	15.1	12.2
C_7	36.6	33.9
C_8	18.9	19.6
C_9	20.4	23.5
C_{10}	4.4	5.6
C_{11}	2.8	3.8
C_{12}	0.1	0.1
C_{13}	<0.1	<0.1
C_{14}	<0.1	<0.1

Table S18. Total capital investment breakdown for the downstream VFA catalytic upgrading TEA model.

Process Area		**Purchased Cost**	**Installed Cost**
Upgrading		$824,000	$1,721,000
Hydrodeoxygenation		$725,000	$1,110,000
Utilities and Storage		$151,000	$221,000
		$1,700,000	**$3,052,000**
Additional Piping	4.5%	of ISBL	$127,000
Total Direct Costs (TDC)			**$3,179,000**
Project Contingency	10.0%	of TDC	$318,000
Other Costs (Start-Up, Permits, etc.)	10.0%	of TDC	$318,000
Total Indirect Costs			**$636,000**
Fixed Capital Investment (FCI)			**$3,815,000**
Land			$700,000
Working Capital	5.0%	of FCI	$191,000
Total Capital Investment (TCI)			**$4,706,000**
All costs are in 2016 Dollars			

Table S19. Variable operating cost breakdown for the downstream VFA catalytic upgrading TEA model.

Upstream Operations	**kg/hr**	**Cost**	**$MM/yr (2016$)**
VFA Feed	1004	$0.30/kg	$2.348
Hydrodeoxygenation			
Purchased H_2	24.5	$1.61/kg	$0.312
Utilities and Storage			
Wastewater Treatment COD	55.6	$0.09/kg COD	$0.042
Natural Gas (Boiler)	0.62 MMBtu/hr	$4.12/MMBtu	$0.020
Natural Gas (Hot Oil)	0.13 MMBtu/hr	$4.12/MMBtu	$0.004
Cooling Tower Chemicals	0.01	$3.93/kg	$0.000
Makeup Water	346.2	$0.31/ton	$0.001
Grid Electricity	99.8 kW	$0.0682/kW	$0.054

Table S20. Fixed operating cost breakdown for the downstream VFA catalytic upgrading TEA model.

Labor		**2016 Cost**
Total Salaries		$255,000/year
Labor Burden (90% of salaries)		$229,000/year
Other Overhead	**Calculation**	**2016 Cost**
Maintenance	3% of ISBL	$85,000/year
Property Insurance & Tax	0.7% of FCI	$27,000/year
Total annual fixed costs		$595,000/year

Table S21. VFA fermentation and recovery inputs and equivalent carbon emissions. Resource consumption (i.e., inhibitor, coagulant, flocculant, antifoam, caustic species) and utilities were based technical consultation with Earth Energy Renewables, along with literature, for a representative VFA fermentation and recovery process. Chemical identifies for common coagulant, flocculant, anti-foam, and caustics used in literature were chosen to estimate the carbon intensity. As noted, VFA fermentation and recovery is an emerging technology area under active development. Resource consumption, waste streams, and utilities are anticipated to vary based on the upstream process configuration, waste feedstock composition, technology readiness level, and scale of implementation.

Resource Consumption	**Flow Rate**	**Carbon Intensity**	**Data Source**	**Emissions (kg CO_2e/h)**
Food waste (dry)	2198.9 kg/h	1.77 kg CO_2e/kg of dry food waste	See note[a]	-3897
Coagulant	120.4 kg/h	1.16 kg CO_2e/kg of $AlCl_3$	SimaPro EcoInvent v3.0 (U.S. average electricity)	139.7
Flocculant	2.9 kg/h	2.77 kg CO_2e/kg of PAM	SimaPro EcoInvent v3.0 (U.S. average electricity)	8.1
Anti-foam	17.1 kg/h	0.89 kg CO_2e/kg of PDMS	SimaPro EcoInvent v3.0 (U.S. average electricity)	15.2
Caustic	97.7 kg/h	2.1 kg CO_2e/kg of NaOH	GREET1 2019_enzymes_yeasts	205.1
Waste Streams	**Flow Rate**	**Carbon Intensity**	**Data Source**	**Emissions (kg CO_2e/h)**
Salt solids (disposal)	43.0 kg/h	--	--	--
Precipitating carbonates (disposal)	50.1 kg/h	--	--	--
Biosolids (dry basis)	393.4 kg/h	--	--	--
Utilities	**Flow Rate**	**Carbon Intensity**	**Data Source**	**Emissions (kg CO_2e/h)**
Natural gas	22.1 MMBtu/h	13.1 kg CO_2e/MMBtu	GREET1 2019_NG (stationary use)	289.9
Nitrogen	74.1 kg/h	--	--	--
Wastewater	83.0 kg/h	--	--	--
Electricity	664 kWh	0.48 kg CO_2e/kWh	GREET1 2019_U.S. average grid	317.3
CO_2 Outputs	**Flow Rate**	**Carbon Intensity**	**Data Source**	**Emissions (kg CO_2e/h)**
Digestions gases	1154 kg/h	--	--	--
Calculated with 54% CO_2	626 kg/h	--	--	--
Exhaust CO_2	20 kg/h	--	--	--
Natural gas CO_2	1153 kg/h	--	--	1153.1
			TOTAL	**-1768.0**

[a] Exhibit 1-51. Documentation for GHG emissions and energy factors used in the waste reduction model (WARM): Organic materials chapters. May 2019. The food waste is otherwise landfilled with LFG recovery and electricity generation. 2) Moisture is calculated based on the ratio of dry weight to wet weight in Exhibit 1-50 (c), i.e., 1- 0.27/(1+0.27)=0.78

Table S22. VFA catalytic upgrading inputs and equivalent carbon emissions based on the downstream Aspen process modeling used in this study.

Resource Consumption	**Flow Rate**	**Carbon Intensity**	**Data Source**	**Emissions (kg CO_2e/h)**
Hydrogen	24.5 kg/h	11.71 kg CO_2e/kg of H_2	GREET_hydrogen, B274 and C275). LHV: 290 Btu/ft^3 and density 2.6 g/ft^3 from fuel-spec	287.3
Water input	346 kg/h	--	SimaPro EcoInvent v3.0 ((U.S. average electricity)	--
Catalyst ZrO_2	0.011 kg/h	5.0 kg CO_2e/kg of ZrO_2	Hydrolysis process. Journal of Nanoparticle Research 8: 1-9 (36).	8.1
Catalyst 3 wt% Pt/3	0.014 kg/h	6.60 kg CO_2e/kg of Pt/gamma Al_2O_3	GREET 2019. Pyrolysis_IDL. Cells S278-280	15.2
Utilities	**Flow Rate**	**Carbon Intensity**	**Data Source**	**Emissions (kg CO_2e/h)**
Natural gas	0.75 MMBtu/h	13.1 kg CO_2e/MMBtu	GREET1 2019_NG. Note stationary use.	289.9
Electricity	100 kWh	0.48 kg CO_2e/kWh	GREET1 2019_U.S. average grid	317.3
Air Emissions	**Flow Rate**	**Carbon Intensity**	**Data Source**	**Emissions (kg CO_2e/h)**
CO_2 biogenic	260 kg/h	--	--	--
CO_2 fossil	39 kg/h	--	--	39
			TOTAL	**384.2**

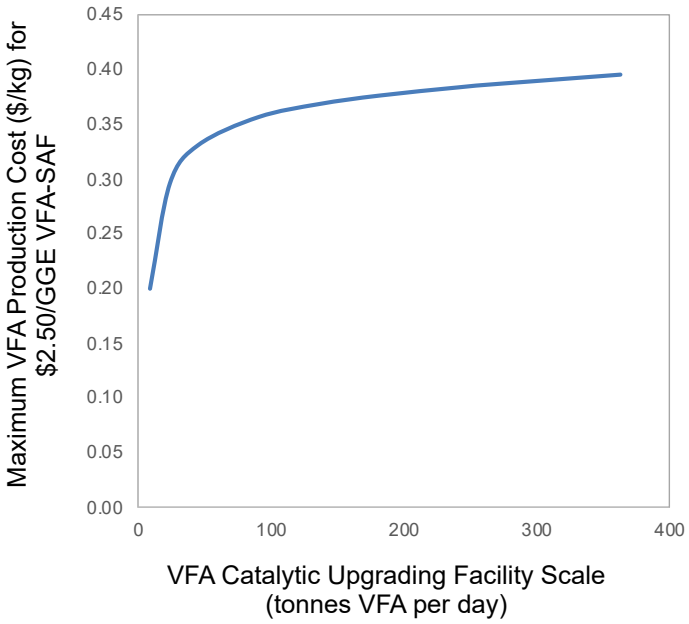

Figure S19. Maximum VFA production cost per kg that will enable $2.50/gallon gasoline equivalent (GGE) of VFA-SAF versus the scale of the VFA catalytic upgrading facility without greenhouse gas reduction credits from the LCFS of other market subsidies. VFA catalytic upgrading scale can increase due to centralized catalytic processing that is decoupled from wet waste fermentation.

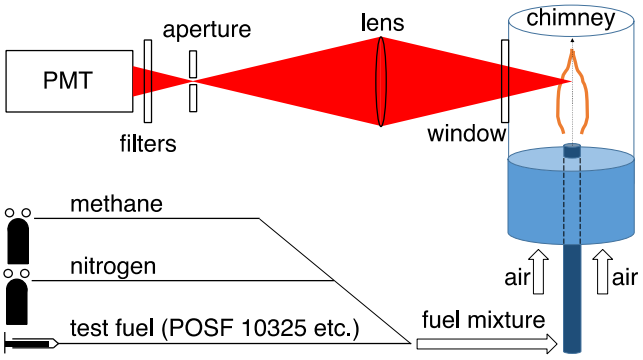

Figure S20. A schematic diagram of the experimental apparatus for measuring sooting tendency.

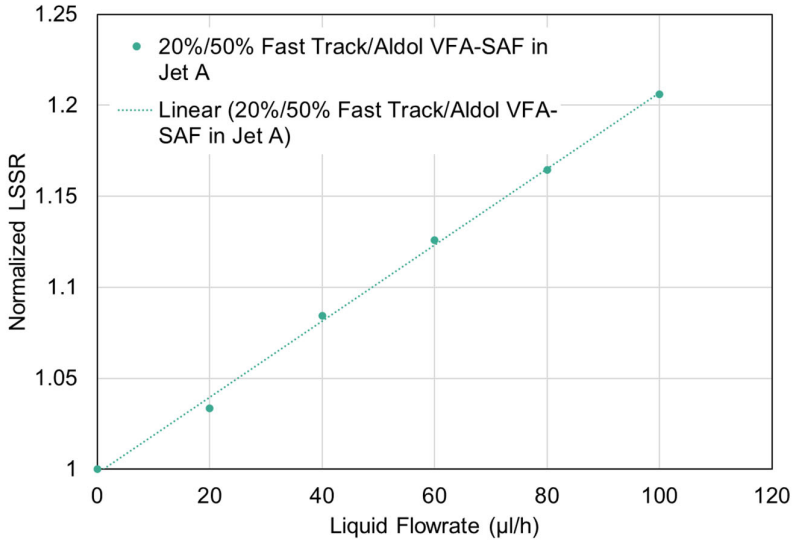

Figure S21. LSSR signals measured for a series of flames doped with varying flowrates of the 20%/50% Fast Track/Aldol Cond. VFA-SAF blend. The signals are normalized to the undoped methane/air flame (liquid flowrate = 0). The dashed line is a least-squares linear fit to the data points.

Section S3: References for Supplemental Information

1. Atasoy M, Owusu-Agyeman I, Plaza E, & Cetecioglu Z (2018) Bio-based volatile fatty acid production and recovery from waste streams: Current status and future challenges. *Bioresource Technology* 268:773-786.

2. Fasahati P & Liu J (2014) Techno-economic analysis of production and recovery of volatile fatty acids from brown algae using membrane distillation. *Computer Aided Chemical Engineering*, eds Eden MR, Siirola JD, & Towler GP (Elsevier), Vol 34, pp 303-308.

3. Granda CB, Holtzapple MT, Luce G, Searcy K, & Mamrosh DL (2009) Carboxylate Platform: The MixAlco Process Part 2: Process Economics. *Applied Biochemistry and Biotechnology* 156(1):107-124.

4. Nelson RSP, D.J.; Karp, E.M.; Beckham, G.T.; Salvachúa, D. (2017) Mixed Carboxylic Acid Production by Megasphaera elsdenii from Glucose and Lignocellulosic Hydrolysate. *Fermentation* 3(10).

5. Carvajal-Arroyo JM*, et al.* (2020) Production and extraction of medium chain carboxylic acids at a semi-pilot scale. *Chemical Engineering Journal*:127886.

6. Saboe PO*, et al.* (2018) In situ recovery of bio-based carboxylic acids. *Green Chemistry* 20(8):1791-1804.

7. Pham TN, Shi D, & Resasco DEJJoc (2014) Reaction kinetics and mechanism of ketonization of aliphatic carboxylic acids with different carbon chain lengths over Ru/TiO2 catalyst. 314:149-158.

8. Gaertner CA, Serrano-Ruiz JC, Braden DJ, Dumesic JAJI, & research ec (2010) Ketonization reactions of carboxylic acids and esters over ceria− zirconia as biomass-upgrading processes. 49(13):6027-6033.

9. CatCost (2020) Version 1.0.4, National Renewable Energy Lab: Golden, CO, USA; https://catcost.chemcatbio.org.

10. Baddour FG, Snowden-Swan L, Super JD, & Van Allsburg KM (2018) Estimating Precommercial Heterogeneous Catalyst Price: A Simple Step-Based Method. *Organic Process Research & Development* 22(12):1599-1605.

11. Davis RE*, et al.* (2018) Process Design and Economics for the Conversion of Lignocellulosic Biomass to Hydrocarbon Fuels and Coproducts: 2018 Biochemical Design Case Update; Biochemical Deconstruction and Conversion of Biomass to Fuels and Products via Integrated Biorefinery Pathways. (United States).

12. Yang X*, et al.* (2019) Hydrodeoxygenation (HDO) of Biomass Derived Ketones Using Supported Transition Metals in a Continuous Reactor. *ACS Sustainable Chemistry & Engineering* 7(17):14521-14530.

13. Huo X*, et al.* (2019) Tailoring diesel bioblendstock from integrated catalytic upgrading of carboxylic acids: a "fuel property first" approach. *Green Chemistry* 21(21):5813-5827.

14. Borgna A, Garetto TF, Monzón A, & Apesteguía CR (1994) Deactivation model with residual activity to study thioresistance and thiotolerance of naphtha reforming catalysts. *Journal of Catalysis* 146(1):69-81.

15. Chang JR & Chang SL (1998) Catalytic Properties of γ-Alumina-Supported Pt Catalysts for Tetralin Hydrogenation: Effects of Sulfur-Poisoning and Hydrogen Reactivation. *Journal of Catalysis* 176(1):42-51.

16. Guenin M*, et al.* (1987) Resistance to sulfur poisoning of metal catalysts: Dehydrogenation of cyclohexane on PtAl2O3 catalysts. *Journal of Catalysis* 105(1):144-154.

17. Striebich RC, Motsinger MA, Rauch ME, Zabarnick S, & Dewitt M (2005) Estimation of Select Specification Tests for Aviation Turbine Fuels Using Fast Gas Chromatography (GC). *Energy & Fuels* 19(6):2445-2454.

18. ASTM (2019) D1322 Standard Test Method for Smoke Point of Kerosene and Aviation Turbine Fuel.

19. Yang Y, Boehman AL, & Santoro RJ (2007) A study of jet fuel sooting tendency using the threshold sooting index (TSI) model. *Combustion and Flame* 149(1):191-205.

20. Haas FM, Qin A, & Dryer FL (2014)?Virtual? Smoke Point Determination of Alternative Aviation Kerosenes by Threshold Sooting Index TSI) Methods. *50th AIAA/ASME/SAE/ASEE Joint Propulsion Conference,* AIAA Propulsion and Energy Forum, (American Institute of Aeronautics and Astronautics).

21. McEnally CS & Pfefferle LD (2007) Improved sooting tendency measurements for aromatic hydrocarbons and their implications for naphthalene formation pathways. *Combustion and Flame* 148(4):210-222.

22. Das DD, St. John PC, McEnally CS, Kim S, & Pfefferle LD (2018) Measuring and predicting sooting tendencies of oxygenates, alkanes, alkenes, cycloalkanes, and aromatics on a unified scale. *Combustion and Flame* 190:349-364.

23. Das DD*, et al.* (2017) Sooting tendencies of diesel fuels, jet fuels, and their surrogates in diffusion flames. *Fuel* 197:445-458.

24. Mensch A, Santoro RJ, Litzinger TA, & Lee SY (2010) Sooting characteristics of surrogates for jet fuels. *Combustion and Flame* 157(6):1097-1105.

25. McEnally CS*, et al.* (2019) Sooting tendencies of co-optima test gasolines and their surrogates. *Proceedings of the Combustion Institute* 37(1):961-968.

26. Humbird D*, et al.* (2011) Process Design and Economics for Biochemical Conversion of Lignocellulosic Biomass to Ethanol: Dilute-Acid Pretreatment and Enzymatic Hydrolysis of Corn Stover. (United States).

27. Bhatt AH & Tao L (2020) Economic Perspectives of Biogas Production via Anaerobic Digestion. *Bioengineering* 7(3).

28. Skaggs RL, Coleman AM, Seiple TE, & Milbrandt AR (2018) Waste-to-Energy biofuel production potential for selected feedstocks in the conterminous United States. *Renewable and Sustainable Energy Reviews* 82:2640-2651.

29. Hafenstine GR*, et al.* (2020) Single-phase catalysis for reductive etherification of diesel bioblendstocks. *Green Chemistry* 22(14):4463-4472.

30. Huq NA*, et al.* (2019) Performance-advantaged ether diesel bioblendstock production by a priori design. *Proceedings of the National Academy of Sciences* 116(52):26421.

31. Davis R, Wiatrowski M, Kinchin C, & Humbird D (2020) Conceptual Basis and Techno-Economic Modeling for Integrated Algal Biorefinery Conversion of Microalgae to Fuels and Products. 2019 NREL TEA Update: Highlighting Paths to Future Cost Goals via a New Pathway for Combined Algal Processing. (United States).

32. Hannon JR*, et al.* (2020) Technoeconomic and life-cycle analysis of single-step catalytic conversion of wet ethanol into fungible fuel blendstocks. *Proceedings of the National Academy of Sciences* 117(23):12576.

33. Zhang L, Butler TL, & Yang B (2020) Recent Trends, Opportunities and Challenges of Sustainable Aviation Fuel. *Green Energy to Sustainability*), pp 85-110.

34. Smagala TG*, et al.* (2013) Hydrocarbon Renewable and Synthetic Diesel Fuel Blendstocks: Composition and Properties. *Energy & Fuels* 27(1):237-246.

35. Fioroni G*, et al.* (2019) Screening of Potential Biomass-Derived Streams as Fuel Blendstocks for Mixing Controlled Compression Ignition Combustion. (SAE International).

36. Osterwalder N, Capello C, Hungerbühler K, & Stark WJ (2006) Energy Consumption During Nanoparticle Production: How Economic is Dry Synthesis? *Journal of Nanoparticle Research* 8(1):1.